UNIVERSIDADE DE LISBOA
FACULDADE DE CIÊNCIAS
DEPARTAMENTO DE FÍSICA

Study of Venus' Atmospheric Dynamics using Doppler Velocimetry Techniques and VLT/UVES Data

Tiago André Bret Barreiros

Mestrado em Física e Astrofísica

Dissertação orientada por:
Prof. Dr. Pedro Machado (FCUL, IA)

2025

Abstract

In this thesis the goal is to measure the winds of Venus's fast rotating atmosphere through the Doppler Velocimetry technique using the high resolution spectrograph UVES on the VLT.

Despite being the closest planet to Earth, the scientific community still do not fully understand how did Venus acquire the characteristics it has today, namely its atmospheric dynamics. Venus is a slow rotating planet with a fast rotating atmosphere, this contrast is not yet well explained, we still do not know how the fast rotation was established and how it is maintained over time.

Measuring and monitoring the velocity of the winds in the rotating atmospehre will help us progress towards answers. We will repeat the same set of procedures from previous studies (Pedro Machado et al. (2012); Pedro Machado (2014)) but using a new set of more recent data from the UVES. The high spectral resolution from UVES and its wide spectral range will allow us to measure in detail the Doppler shift from every Fraunhofer line that is reflected by the fast moving particles in the upper layer of Venus's clouds.

The observations use a long slit that is placed perpendicularly to the rotation axis in specific latitude circles, since the zonal wind is practically independent from longitude, with the exception of local oscillations, each observation will have a nearly constant wind velocity. In this thesis we will only display the results from one exposure, however, in further work, a latitudinal profile will be assembled using all exposures from all slit positions, and local oscillation patterns will be studied.

This method is the only way we can measure in detail and with accuracy the velocity winds of Venus's zonal rotation since corrently there is no space probes orbiting Venus and the only way we can observe it is from ground.

We successfully managed to obtained and measured the absolute velocity values of atmospheric winds, which were consistent with results from previous studies, concluding that the Doppler velocimetry tecnique is an effective method for studying atmospheric dynamics.

Keywords: Venus, Doppler velocimetry, Retrograde zonal superrotation, High resolution spectroscopy, Zonal winds

Resumo

Vénus sempre foi um planeta que despertou ao ser humano bastante curiosidade. Apesar de ser o nosso vizinho mais próximo, pouco se sabe sobre ele, sempre foi de muito difícil acesso e sempre nos deixou com grandes questões e a cada vez que um dos seus segredos era revelado, mais dúvidas surgiam sobre ele.

É talvez o planeta do nosso sistema solar mais semelhante à Terra, quer em próximidade ao Sol, quer em grandezas físicas como o raio, a densidade ou a massa. Daí ser muitas vezes apelidado do nosso planeta "irmão". No entanto, quanto mais navegamos as profundezas deste misterioso planeta mais diferenças encontramos entre os dois planetas "irmãos". E começamos a perceber que se calhar este nosso vizinho que à primeira vista seria tão semelhante a nós, afinal pode ser mais visto como um planeta desértico, inóspito e árido, mais parecido com a concepção humana de inferno e extremamente contrastante com o nosso planeta Terra.

Vénus está bastante habituado a ser observado pelo ser humano. Desde os tempos antigos que os povos se deslumbravam com as suas fases e brilho intenso, teve já muitos nomes e até foi lhe dado o título divinal. Mais recentemente, são já várias as missões espaciais que se projetaram em direção a este corpo celeste e muitas se atreveram a cruzar as suas fronteiras atmosféricas, dentre elas tivemos o *Mariner Programm*, o *Venera Programm*, a *Pioneer Venus mission*, a sonda *Magellan*, a *Venus Express*, desenvolvida pela ESA e a *Akatsuki mission*, da agência espacial japonesa. Infelizmente, esta última missão teve de ser interrompida prematuramente, de modos que, atualmente, não existe nenhuma sonda espacial a orbitar Vénus. A próxima será a *EnVision*, também desenvolvida pela ESA e está agendada para 2031. Portanto, estamos neste momento num período de tempo de alguns anos em que apenas é possível observar e estudar Vénus a partir da superfície terrestre.

Estas inúmeras tentativas de aproximação ao nosso planeta vizinho permitiram-nos descobrir e perceber melhor como Vénus funciona por baixo do seu véu opaco que esconde todas as suas ações. Estas corajosas iniciativas revelaram-nos que a atmosfera de Vénus é super densa, com pressões altíssimas, e que é a mais quente do sistema solar, mesmo não sendo o planeta mais próximo do Sol. Estas condições atmosféricas adversas devem-se maioritariamente ao elevadíssimo efeito de estufa que lá existe que é principalmente causado pelo dióxido de carbono que corresponde à quase totalidade dos gases atmosféricos. Além disso, Vénus apresenta não ter campo magnético, assim como magnetosfera, nem movimento tectónico de placas. Isto é devido à rotação muito lenta sobre si próprio (que é também feita no sentido contrário aos demais planetas), que o faz ter o dia mais longo do Sistema Solar, mais longo até que o próprio ano. A superfície está, no entanto, num constante estado de erupção geral e global, o que faz com que seja sempre muito recente e seja rara a presença de crateras. O mais interessante, e que nos desperta mais curiosidade, é o facto de que apesar do planeta ser muito lento na sua rotação, descobriu-se que a sua atmosfera é extremamente rápida. Ou seja, temos uma atmosfera super rápida num corpo celeste super lento, claramente uma surpresa de que ninguem estava à espera.

Esta atmosfera é composta principalmente por três camadas: troposfera, mesosfera e termosfera. Na

metade superior da troposfera temos uma densa e extensa camada de nuvens feitas de ácido sulfúrico. O limite superior desta camada (mais ou menos 70km de altitude) dita o início da mesosfera. É nesta região da atmosfera que nós nos vamos focar nesta tese pois, acontece que, a todo o instante, raios de luz que vêm do Sol embatem nas partículas que compõem as camadas superiores das nuvens de Vénus; estas partículas, que viajam a alta velocidade ao redor de Vénus, espalham (*scatter*) e refletem esses fotões em todas as direções, incluindo a direção do observador, a nossa. Como no momento do redirecionamento as partículas estão em movimento, elas induzem um desvio de Doppler no comprimento de onda dos fotões que captamos. Através desse desvio de Doppler é possível calcular a velocidade a que a partícula se deslocava quando redirecionou o fotão. A esta técnica chamamos velocimetria de Doppler e através deste método conseguimos medir as velocidades dos ventos na atmosfera de Vénus.

Em Vénus existem três principais dinâmicas atmosféricas: a circulação de Hadley (com uma célula em cada hemisfério, na zona de menor altitude, que leva o ar do equador até aos polos), a circulação do ponto subsolar para o ponto antisolar (dominante na camada mais externa, causada pelo desiquilíbrio térmico entre a metade diurna e noturna de Vénus, devido à lenta rotação do globo) e a super rotação zonal (rotação atmosférica paralela ao equador com elevada velocidade). É nesta última circulação que nós nos queremos focar. O objetivo é medir as velocidades dos ventos zonais que circulam horizontalmente ao vedor de Vénus na zona por cima da camada de nuvens. Vamos usar o método da velocimetria de Doppler através de observações feitas a partir da superfície terrestre. Este método beneficia bastante de uma grande resolução espectral, crucial para se conseguir medir todos os desvios nos comprimentos de onda, e também de uma ampla cobertura espectral para conseguir detetar todas as linhas solares de Fraunhofer. Com base nestas condições, recorremos ao UVES, um espectrógrafo de alta resolução implementado no VLT, no deserto do Atacama. A grande área de recolha do telescópio (isto é, o seu grande diâmetro) e local onde foi construído (sem poluição atmosférica) também contribuem para melhorar as condições de observação.

O vento zonal é praticamente independente da longitude, salvo certas oscilações e variações locais, dependendo então apenas da latitude. As observações que vamos usar foram feitas com recurso a uma slit longa colocada perpendicularmente ao eixo de rotação de Vénus. A slit é colocada em várias posições mas em cada uma delas a latitude é a mesma para toda a slit, portanto, para cada observação temos a slit a incidir numa latitude específica, e então, em cada exposição o vento é aproximadamente constante. Estamos a utilizar observações realizadas em 2018 em três dias diferentes (20 de Agosto, 29 de Agosto e 3 de Setembro), num total de 45 observações que foram colocadas em várias posições de latitude constante. Nesta tese, revelo os cálculos do vento zonal para apenas uma dessas 45 observações, no entanto, num futuro próximo tenciono divulgar os resultados para a totalidade das observações, de modo a fornecer uma visão mais ampla e geral da variação dos ventos zonais ao longo das diversas latitudes, desenvolvendo então um perfil latitudinal e podendo até estudar a presença de oscilações e variações locais.

Pretendo ainda comparar os resultados com anteriores estudos que seguiram os mesmos métodos e que usaram os mesmos instrumentos com as mesmas configurações para medir os ventos em Venus (Pedro Machado et al. (2012); Pedro Machado (2014)), e outros que usaram a distinta porém complementar técnica de *cloud tracking*, que rastreia as nuvens na atmosfera de Vénus a partir de sondas que o estejam a orbitar. Apesar desta tese ser uma réplica de estudos já efetuados utilizando novos dados, esta técnica revela-se muito importante num período onde a observação de Vénus é apenas possível a partir da superfície terrestre, e revela-se também muito versátil pois foi já aplicada em observações de outros corpos no Sistema Solar e quem sabe, poderá ser aplicada também no futuro em observações de exoplanetas.

Palavras chave: Vénus, Velocimetria de Doppler, Superrotação zonal retrógrada, Espectroscopia de

alta resolução, Ventos zonais

Acknowledgements

First of all, I want to thank the Faculty of Sciences of the University of Lisbon for providing me with these five years of quality education, Bachelor's and Master's degrees, giving me the conditions and foundations to progress and evolve as a student and young researcher, specializing in recent years in the field of astrophysics, a component of physics very well represented in this great institution. From early on I decided that this would be the place where I would pursue my higher education, and I hope that our relationship will continue for many more years.

Obviously, I want to thank my supervisor, Prof. Dr. Pedro Machado, for giving me the opportunity and honor of working with him. From the moment I took my first course with him, I realized he would be the role model and the path to follow, not only in a possible professional career as a scientist but also in the way of teaching and disseminating science, always managing to spark the curiosity of each student in a friendly and accessible way, within a horizontal relationship. I hope to continue learning and collaborating with you for much longer.

I can not help to thank Rafael Rianço Silva for always being available to help me and for always having the patience to clarify and answer all my questions and doubts; without him it would have not been possible. It was a pleasure working alongside you, and I hope to do so again. I also want to thank the other members of the planetary troop and the entire IA squad. It is a pleasure and an honor to be part of this team.

To all my friends, especially those who accompanied me daily at Abade Faria and were present throughout this long year, thank you for all the motivation and strength you gave me page after page, words of comfort mixed with sarcasm, and well-deserved breaks for various reasons.

To the two people who made all this possible, thank you Mom and Dad for always giving me all the foundations and tools I needed to grow as a person and to choose who I want to be professionally. I hope one day I can repay everything you have ever done for me, I hope one day I can raise my children as well as you did, and instill in them the same values you did.

Last but not least, I want to thank Joana for always believing in me, for always motivating me, for always giving me strength, for being my biggest fan, for being my greatest support. With you by my side, everything is easier, everything is possible...

Índice

List of Figures **xiii**

List of Tables **xv**

1 Introduction **1**

2 Venus **3**
2.1 Our neighbor planet . . . 3
2.2 Earth's evil twin . . . 4
2.3 Atmospheres of telluric planets . . . 8
2.4 The Venusian Atmosphere . . . 11
2.4.1 Global atmospheric circulation . . . 14
2.5 History of Venus exploration . . . 17

3 Method **21**
3.1 UVES - Ultraviolet-Visual Echelle Spectrograph . . . 21
3.2 Doppler Velocimetry with UVES . . . 24
3.2.1 Doppler Shifts . . . 26
3.3 Data retrieval and algorithm . . . 28
3.3.1 Observational biases . . . 28
3.3.2 The database . . . 31
3.3.3 WIND software package . . . 32
3.3.4 The proposal and the chosen exposure . . . 33
3.3.5 From relative Doppler shifts to absolute velocity winds . . . 34
3.4 Results . . . 36

4 Discussion, conclusions and future work **39**

List of Figures

2.1 A seemingly peaceful view of Venus captured by NASA's Mariner 10 space probe as it flew away from Venus in 1974. However, Venus is a world of extreme temperatures, overwhelming atmospheric pressures and corrosive acid clouds, contrary to its serene appearance. (Image: NASA/JPL-Caltech website). 3

2.2 Computer-synthesized image of Venus from a mosaic of radar altimetry images obtained by the Magellan spacecraft during its first mapping cycle of the planet. (Image: NASA/JPL website). 5

2.3 Formation of Venus's magnetosphere by molecule ionization in the outer atmosphere. Note for the loss of H^+ in the night hemisphere, i.e. in the region without magnetosphere. (Image: ESA website). 6

2.4 Three-dimensional image of Venus's surface, synthesized from radar images obtained by the Magellan spacecraft. On the left of the image there is a volcano with about 3 km high (Gula). The lava flows across the fractured plains are visible in the foreground. (Image: NASA/JPL website). 7

2.5 Relative composition of Venus's atmosphere with relative abundances of minor species at the right side. (Figure: NASA website). 8

2.6 The atmospheric global circulation of Solar System's terrestrial-type planets. From Pedro Machado (2014). 10

2.7 Averaged thermal profile with altitude (a) and pressure (b) plus condensable species for Venus, Earth and Mars. Figures from Pedro Machado (2014). 11

2.8 Image of Venus taken by the Pioneer Venus's space probe in ultraviolet in 1979. The presence of an Y-shaped cloud pattern is visible. (Image: NASA/JPL website). 12

2.9 The cycle of SO_2 in Venus's atmosphere and respective radiative interactions. From Pedro Machado (2014). 13

2.10 Illustration of Venus's atmospheric structures and interactions. From Pedro Machado (2014). 14

2.11 Illustration of Venus's global atmospheric circulation. From Pedro Machado (2014). . . . 15

2.12 Planetary atmosphere motion for Earth (left) and Venus (right) at large-scale: different types of circulation patterns are visible in relation to latitude, altitude and local time. From Pedro Machado (2014). 16

2.13 Various Venera program landings in the Venusian surface throughout different missions. (Image: Russian Academy of sciences). 18

3.1 ESO's VLT facility in Paranal, in Chile's Atacama desert, where UVES is located. (Image: ESO's website). 21

3.2 UVES characteristics and observing capabilities. From UVES manual, European Southern Observatory (2007). 22
3.3 Image from the UVES slit viewer camera, showing the spectroscopic slit on the disc of Venus (a), from Pedro Machado (2014). View of a portion of a spectral order obtained in the DS9 software (b). The horizontal direction corresponds to the spatial variation and the vertical direction to the spectral variation. We can see the different portions of the slit (in pixels) that take different parts of the disc: the red band corresponds to the dayside, the mixture of yellow, orange and red pixels corresponds to the nightside and outside the disc, the mixture of green and blue pixels corresponds to the inactive window of the slit. 23
3.4 UVES CCDs properties measured. From UVES manual, European Southern Observatory (2007). 24
3.5 Overall detection effectiveness of UVES + detectors + 3 UT2 mirrors, corrected for the contribution of the atmosphere, for the different cross-dispersers (a). Mean resolving power R (in 1000) as function of the slit width (b). From European Southern Observatory (2007) 26
3.6 Illustration of how to obtain radial velocity using only the shift of one spectral line. From Pedro Machado (2014) 26
3.7 A UVES echellogramme example showing each step to obtain the desire spectra. First, in (a), we have the raw unprocessed echellogramme with the spectral orders. Next, in (b), we took part of one of these spectral orders and zoomed it to look at the absorption lines visible (dark vertical bands). In (c) we can see that each order contains a stack of 61 spectra, with each spectra corresponding to one pixel in the active window of the slit. Then, in (d), each spectrum is divided into 16 orders for the MIT detector and 23 orders for the EEV. Finally, in (e), the ends of each component are joined to get the final example spectrum from one order and one location in Venus's disc. From Pedro Machado et al. (2012) 29
3.8 Representation of the Doppler effect (a), the dotted arrow in the sub-terrestrial point represents the redshift in the absorption of solar radiation and the dashed arrow at the sub-solar point represents the blueshift in the emission of solar radiation towards the observer, thin arrows represent the direction of zonal wind motion. Iso-lines for the geometric projection factor (b) and Young effect (d). Respective exemple behaviors for the de-projection factor (c) and Young effect (e) as function of longitude. From Pedro Machado et al. (2012) and Pedro Machado (2014). 30
3.9 Observation proposal made for this set of observations with UVES that consisted of 13 different slit positions, perpendicular to Venus's rotation axis (PP), covering the latitude parallels from -60º to +60º, with a separation of 10º (corresponding to separations of 2"). From European Organisation for Astronomical Research in the Southern Hemisphere (2017). We consider the $K9$ to be in the latitude slit position of 20^o North. In this image we can see the total slit window of 20 arcseconds, but we only get results from the active window which as only 12 arcseconds. 34
3.10 Zonal wind versus longitude for the 9^{th} observation (K9) made at August 20^{th} 2018 with the spectroscopic slit parallel to the equator. We are only considering the MIT detector. The slit latitude is 20 N and the central slit longitude is 46.785 E. 37
3.11 Slit's position scheme on the planetary disc, with an apparent radius of 12.66", for the K9 case. It is only shown the active window of the slit on the dayside with 12 arcseconds. 38

List of Tables

3.1 North Pole position angle, apparent radius of Venus, latitude of sub-solar point and phase angle at the time of the K9 exposure. From NASA Jet Propulsion Laboratory (2024) . . 34

3.2 Table showing the relative Doppler shift obtained from the algorithm and respective error, we also displayed the slit region by pixel and the corresponding place in the planetary disc. The shift error increase along the slit is due to the curvature of the planet, pixels closer to the limb detect radiation that passes through a more extensive layer of the atmosphere and therefore undergoes greater scattering 35

3.3 Table showing the Longitude, Young effect and De-projection factor given for each pixel in the dayside 36

3.4 Summary of the geometry and circunstances of the observations. The integration time for all exposures was 1 second. Lat and Long are the coordinates of the slit's central point on the disc and their values are affected by the VLT/UVES nominal pointing and offset uncertainty, with a total uncertainty of 0.14". 36

3.5 Latitude covered and mean zonal wind velocity measured for the K9 exposure with the PP geometry. Std. Dev. is the standard deviation of the weighted mean. The latitude is given for the slit center with an uncertainty of 1.2º; the 0.3"-slit covers a latitude band of 2.4º at disc center. 38

Chapter 1

Introduction

Since the beginning of human space exploration, Venus was the first planet and celestial body other than the Moon to capture our attention and curiosity, becoming the chosen target for many of the first probes and spacecraft developed. However, it was soon realized that the interior of this planet was very difficult to access, unlike our neighbor, Mars. It seemed that humanity was doomed to only contemplate this goddess-named planet from the outside. Few probes and atmospheric balloons managed to penetrate the dense atmosphere and survive the harsh atmospheric conditions of high pressure and temperature. Despite being named after the Roman goddess of love, Venus was quickly associated with a desert and hellish planet. All these conditions, initially unpredictable, sparked even more interest and curiosity in the scientific community. How did Venus get to this state? What happened? These questions become even more ironic when we begin to compare this planet to Earth. Venus is the closest planet to us and has the most similar physical characteristics (size, density, etc.). Since all planets originated from the same cloud of gas and dust, with the same initial compositions, when the Solar System formed, new questions begin to arise. How could Venus become so different from Earth? At what point did this happen? And when we begin to study the runaway greenhouse effect that occurs on Venus, which is the main responsible for the extremely high temperatures, we ask ourselves: could Earth one day become like Venus? These questions can only be answered through successive studies and initiatives that allow us to analyze and monitor the dynamics occurring on this neighboring planet, particularly in its atmosphere.

This atmosphere is very intriguing because it rotates very fast around a planet that rotates very slowly. It is the only planet in the Solar System with a counter-rotation and is the slowest of all. This atmosphere also has the strongest and most effective greenhouse effect in the Solar System, making it the planet with the highest temperatures, despite not being the closest to the Sun. All these mysteries deserve investigation. Unfortunately, there are currently no space probes around Venus after the tragic end of the Akatsuki mission. Therefore, the only way we have to study Venus's atmosphere and try to unravel the secrets of its rapid rotation is through ground-based telescopes.

On Venus, the atmosphere's circulation up to the cloud tops is contrasting dramatically with the rotation period of the solid globe. The first is characterised by an increasing zonal wind in the retrograde sense, called the retrograde zonal superrotation (RZS), that circles the planet in 4.4 days at the cloud tops (near 70 km altitude). While the latter takes 243 terrestrial days to make a full rotation. In the mean zonal flow two main large-scale components are superimposed: the solar tide and the traveling four-day wave. The solar tides are forced by solar heating and were initially proposed as the caused to the superrotation of Venus's atmosphere. However, although they seem to dominate the dynamical structure at higher atmosphere layers, this global-scale motion does not provide a satisfactory explanation to the dynamical exchanges in Venus's mesosphere. In order to constrain the mystery around this superrotating atmosphere

mechanism, we will use the Doppler velocimetry technique (a tecnique that measures the shifts between the absorption lines of spectra), that already proved its effectiveness in Pedro Machado et al. (2012) and Pedro Machado (2014), to retrieve zonal and meridional wind velocities on Venus's dayside, their spatial variability and yield a latitudinal profile of the wind velocity (European Organisation for Astronomical Research in the Southern Hemisphere, 2017).

The telescope choice justification lies on the fact that the combination of UT2 and UVES (telescope and instrument) is the only long slit spectrograph inserted in a high performance telescope that can provide very high-resolution spectra (on the order of 10^5) of the back-scattered solar radiation on Venus's atmosphere. We need this high level of resolving power because the shifts that we want to measure are much smaller than the actual line width. Using our Doppler velocimetry technique (Pedro Machado et al., 2012), we are hopping to retrieve wind velocities with a precision with less then 10 m/s. This high precision is indispensable to the study of the latitudinal profile of the meridional wind, relevant to the constrain of Venus's atmospheric dynamics and to detect the presence of atmospheric planetary waves. The UVES/VLT combination possesses the capabilities to perform simultaneous wind profles, that require high signal-to-noise ratios with high spectral and spatial resolution unreachable by any other instrument (European Organisation for Astronomical Research in the Southern Hemisphere, 2017).

Taking advantage of the obtained high-resolution spectra, the goal is to provide direct absolute wind measurements in Venus's dayside mesosphere. We are hopping to measure the latitudinal profile of the meridional and zonal winds at the cloud top layer, and to detect the presence of wave motions, this profile will also allow to judge the relative importance of the angular momentum transport by the Hadley circulation (a cell that carries air from the equator to the poles). The Doppler measurements will provide direct wind measurements, allowing a direct comparison with results obtained using the cloud-tracking technique, for example, by the now-defunct Akatsuki space probe, which also measures winds at cloud level. (European Organisation for Astronomical Research in the Southern Hemisphere, 2017).

Chapter 2

Venus

2.1 Our neighbor planet

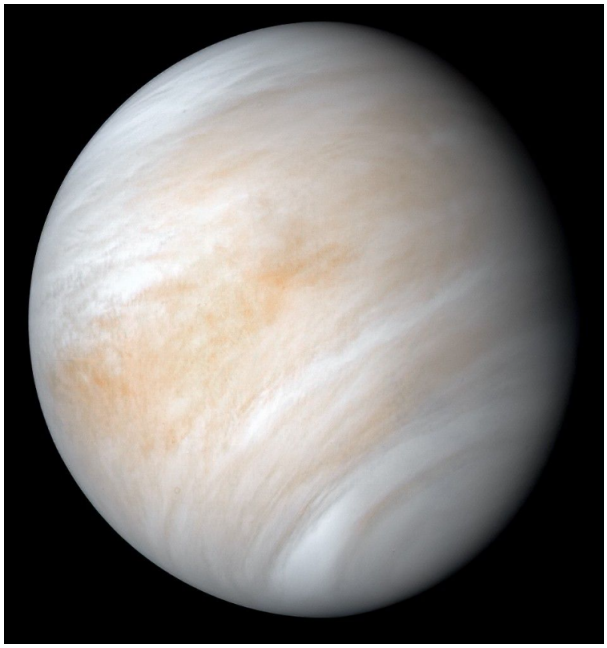

Figure 2.1: A seemingly peaceful view of Venus captured by NASA's Mariner 10 space probe as it flew away from Venus in 1974. However, Venus is a world of extreme temperatures, overwhelming atmospheric pressures and corrosive acid clouds, contrary to its serene appearance. (Image: NASA/JPL-Caltech website).

Venus is our planet next door in this large condominium that is the Solar System. The second closest to the Sun and the closest to ourselves. Usually it is the third brightest celestial body in our sky, after obviously the Sun and Moon, reaching an apparent magnitude of about -4.6 (Pedro Machado, 2014). Viewed from Earth, Venus is always very close to the Sun; there is a small angular distance between them, as its orbit is interior to ours, therefore it is most commonly seen as a morning (before sunrise) or evening (after sunset) "star" (Cornish, 2025). This fact also makes Venus very difficult to observe in quality, as the time window is always very short and the observation of bodies lower in the sky usually results in more turbulence, poorer *seeing* and higher airmass (Abel, 2017).

The terms "star" for the morning and the evening come from a long time ago. Since the Babylonians and ancient Egyptians, it was thought that they were two different bodies with two different names. It was only in the 4th century BC that Pythagoras realized that these two stars were after all part of the

same celestial body (ESO Education Office, 2004). And it was Ptolemy, in the *Almagesto*, the first to place Venus between Earth and the Sun, despite supporting the geocentric model (Kak, 1996). It was the Romans who gave it the name we all call it today, symbolizing the Goddess of love, beauty, and fertility, equivalent to Aphrodite in Greek mythology (National Aeronautics and Space Administration, 2025).

In the modern era, the first to observe Venus in detail, for scientific studies and using pioneering observation equipment was Galileo Galilei. In 1610, he started pointing his refractor to Venus and he was even able to observe its phases, which was at the time an important step in the fight for the heliocentric model, which highlighted that era. Not long after, the passage of Venus behind the Sun dictated the victory of Copernicus' theory. Subsequent observations made by several astronomers, such as Gian Domenico Cassini, William Herschel, and Lomonosov, reported the presence of a bright halo around the planetary disc; this was the first evidence that Venus had an atmosphere (Pedro Machado, 2014) (Grinspoon, 1997) (Marov et al., 1998).

Venus is unique in our Solar System because it is the only one that rotates in a retrograde direction; this happens because it has an inclination angle of 177º, rotating upside down. Since both hemispheres receive practically the same amount of radiation throughout the year, we can neglect seasonal variations (Bougher et al., 1997). This high tilt is believed to have been caused by a possible catastrophic impact, somewhat similar to a possible Earth-Thea impact, but even more aggressive, which caused the high tilt and therefore the retrograde rotation (Pedro Machado, 2014).

Another unique characteristic of Venus is that its rotation period around itself (243 Earth days) is greater than its translation period around the Sun (225 Earth days); this makes the day greater than the year (Espaço do Conhecimento UFMG, 2022). However, Venus's solar day, that is, the time it takes for the Sun to pass twice consecutively at the zenith of the same place, results from the combination of rotation and translation movements, giving a solar day of about 117 Earth days, shorter than the year (Pedro Machado, 2014). Despite all this laziness, its atmosphere at the cloud tops circles the planet in 4.4 days, it is called the Retrograde Zonal Superrotation (RZS).

At first glance, we might think that Venus would be the planet most similar to Earth. It is the closest planet to us, with an orbit of only 38 million kilometers away. It is 108 million kilometers from the Sun, which corresponds to 0.72 AU; sunlight takes about 6 minutes to reach Venus and another 2 minutes to reach Earth. In terms of dimensions, it is also the planet most similar to Earth, with a diameter at the equator of 12,104 kilometers, 0.95 times the diameter of Earth. Venus's mass corresponds to 0.815 Earth masses, so the average density is also similar (National Aeronautics and Space Administration, 2025). However, we will see that despite all the similarities, Venus can be almost opposite to Earth, and this plot twist is why it is often called Earth's evil twin.

2.2 Earth's evil twin

Both Earth and Venus have originated from the same cloud of gas and dust; they both have formed at roughly the same time and went through similar debris bombardments in the early years. The amounts of initial radioactive elements and the abundance of volatiles could also have been similar (Pedro Machado, 2014) (Turcotte, 1995). So, despite starting with similar conditions, they followed totally different paths in planetary evolution. Therefore, this makes Venus the best planet to study when we want to compare it to Earth, it is like the one that lost all of its potential, our job is to find out what happened that made these two "twins" so different.

Although in physical and dimensional aspects these two planets seem very similar, when we start to "dive" deep into them, we begin to see immense disparities regarding, for example, the compositions

Figure 2.2: Computer-synthesized image of Venus from a mosaic of radar altimetry images obtained by the Magellan spacecraft during its first mapping cycle of the planet. (Image: NASA/JPL website).

of the atmosphere and soils, the type and intensity of geological events, namely volcanism and plate tectonics, the abrupt differences in temperature and pressure, the type of surfaces and reliefs, and the presence of a magnetic field (Pedro Machado, 2014).

It is important to note that if we introduce the planet Mars into this game of comparisons, it is Earth that comes out defeated, because Venus has much more in common with Mars than with our "blue planet". Both Venus and Mars do not have a magnetic field, although for different reasons, and their atmospheres are very similar. Therefore, perhaps it was Earth that evolved differently from its neighbors and not the other way around. Everything indicates that it was the presence of water that made the difference, because it captured CO_2 from the atmosphere, deposited it on the ocean floor (carbon corals and ocean rocks), released O_2 into the atmosphere and, due to the tectonic movement of subduction (facilitated again by its presence and lubricating action), buried the carbon in the mantle (Pedro Machado, 2024).

But back to Venus, its iron core is proportionally smaller than Earth's, about a third of the planet's for the former and half for the latter, the core is then surrounded by a mantle of incandescent rock and a thinner layer forms an outer rocky crust (National Aeronautics and Space Administration, 2025). This smaller core can be explained by a collision of enormous magnitude, similar to the hypothetical collision between Earth and Thea, but even stronger, so strong that it even tore off part of the core. This collision would also explain the inverted axis and the slow rotation of Venus (Pedro Machado, 2024). So, this could be why Venus does not have a magnetic field. Its absence is crucial because it slows down any dynamics inside the planet, which is therefore much colder and more static. Thus, there is no tectonic movement, only of the crust, so the volcanism is of the shield type (hot spots), the entire surface is in general volcanism all at the same time and the eruption points are always in the same place. Since the surface is very dry and lacking water, any movement on the surface, either due to collisions or magma, creates cracks and fractures in the crust, rather than shaping or deforming it (Pedro Machado, 2014). The absence of a magnetic field also leaves the planet unprotected from the solar winds, making the existence of life even more difficult. However, light from the Sun excites gases from Venus's outermost atmosphere creating the ionosphere, then these ions interact with the Sun's magnetic field carried by the solar wind,

a storm of electrically charged particles at a million kilometers per hour streaming continuously from the Sun, creating or inducing a weak magnetosphere (see Figure 2.3) that involves the planet in an extended teardrop shape as the solar wind blows past Venus and outward into the solar system (National Aeronautics and Space Administration, 2025) (Goody et al., 1975). From there it is possible to observe the escape of ionized hydrogen, due to its low weight, and even oxygen, although in smaller quantities, making it difficult to form essential molecules for life such as H_2O and O_2 (Pedro Machado, 2014).

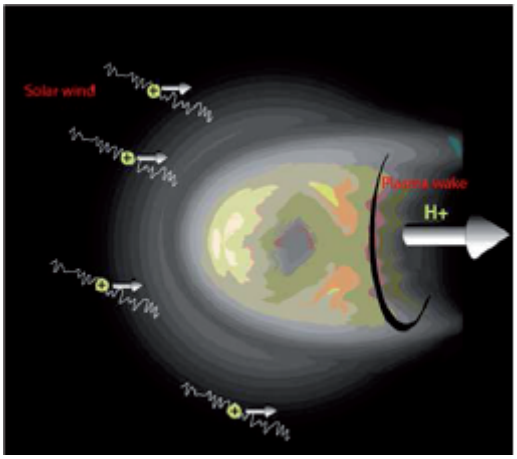

Figure 2.3: Formation of Venus's magnetosphere by molecule ionization in the outer atmosphere. Note for the loss of H^+ in the night hemisphere, i.e. in the region without magnetosphere. (Image: ESA website).

The thermal gradient on Venus is also much smaller, compared to Earth, as the core is colder and the surface is hotter, so the temperature difference between the surface and the core is much smaller; this makes the convective cells in the mantle much less effective, in addition the viscosity of the mantle is greater, again due to the absence of water, which makes their movement slower and more time-consuming and the planet drier. Due to this general volcanism, the surface of Venus is secondary and always very young, not lasting long before being covered again by the molten mantle and renewed (Pedro Machado, 2014) (Pedro Machado, 2024).

The average age of Venus's surface is around 150 million years, with some older areas mixed in. Therefore, any trace of the original surface of Venus has been "erased" by intense volcanism over the years. Venus's surface images have shown a desolate landscape of basaltic rocks and basaltic plains (nearly 80%) chemically eroded with small amounts of soil between them. Throughout it, we find valleys and high mountains filled with a wide variety of volcanic features: shield volcanoes, ring-shaped reliefs (Coronae), and fluvial features (channels that extend for thousands of kilometers in the shape of river deltas) (Pedro Machado, 2014) (Kargel et al., 1994). Most of these geological phenomena are named after women, both real and mythological, such as Ishtar Terra, a rocky plateau area near the north pole that is similar in size to Australia, and Aphrodite Terra, a region the size of the American continent that extends to the equator. One of the largest mountains reaches 11 kilometers in altitude, higher than Mount Everest. It should be emphasized that Venus, after Earth, is the terrestrial planet with the smallest number of impact craters on its surface; this is because, as we have seen, it is constantly being renewed by volcanism, but also because the extremely dense atmosphere disintegrates the vast majority of meteors before they reach the surface (National Aeronautics and Space Administration, 2025).

Other geological features on Venus's surface include (National Aeronautics and Space Administration, 2025):

- A volcanic crater named Sacajawea, after Lewis and Clark's Native American guide

- A deep canyon named Diana after the Roman goddess of the hunt
- Pancake-shaped domes that are flat on top and steep on the sides, up to 62 kilometers wide, probably formed by highly viscous lava flows
- Tick-shaped domes, strange volcanoes with radiating spurs that, seen from above, make them look like their blood-feeding namesakes
- Tesserae, terrain with intricate patterns of ridges and grooves (see Figure 2.4) suggesting that the extreme temperatures cause the rock to behave somewhat like peanut butter under a thin, thick layer of chocolate on Venus.

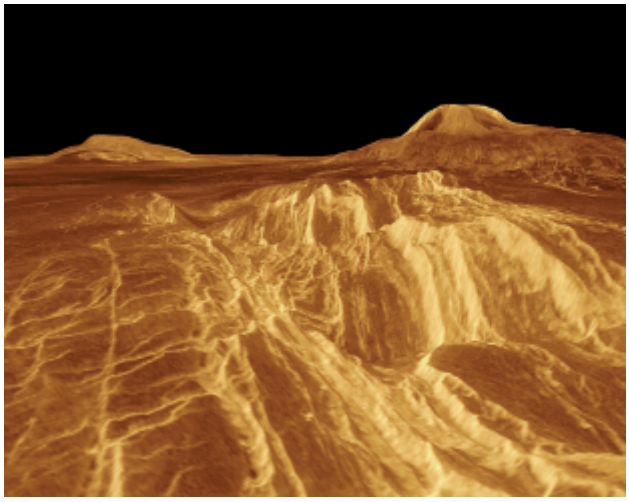

Figure 2.4: Three-dimensional image of Venus's surface, synthesized from radar images obtained by the Magellan spacecraft. On the left of the image there is a volcano with about 3 km high (Gula). The lava flows across the fractured plains are visible in the foreground. (Image: NASA/JPL website).

When we focus on the atmosphere, we can also see huge disparities between Venus and Earth. Starting with the composition (see Figure 2.5): the vast majority of the Venus's atmosphere is composed of carbon dioxide, up to 96.5%; the second most abundant gas, although in much smaller quantities, is nitrogen, reaching nearly 3.5%. Then we have the minor species of gases: sulfur dioxide (150 ppm), argon (70 ppm), water vapor (20 ppm), carbon monoxide (17 ppm), helium (12 ppm) and neon (7 ppm) (Pedro Machado, 2014) (Marcq, Encrenaz, et al., 2006) (Clancy et al., 2012) (Cottini et al., 2012) (Marcq, Bertaux, et al., 2013). Although very different, we can see some similarities between the two atmospheres, starting with the common presence of nitrogen and argon. These two gases are not very reactive, one of them being a noble gas, so it is possible that their current presence on Venus indicates the existence of an ancient atmosphere much more similar to the Earth's that for some reason has been replaced by the current atmosphere with the abrupt increase of carbon dioxide. Its excessive abundance is due to the lack of absorption by the oceans, as on Earth, and the impossibility of surface deposition by chemical reactions between the surface and the atmosphere, since CO_2 is in the supercritical state on the overheated surface. (Pedro Machado, 2014).

For Argon, the absolute amount on both planets is similar, the greater relative presence of Argon in a less heavy atmosphere like Earth compensates for the lower concentration in the massive atmosphere of Venus. As for nitrogen, despite being in a smaller relative quantity, Venus's heavier atmosphere makes it have much more nitrogen in absolute terms than Earth (Williams, 2024). However, it is important to

remember that on Earth, much of the nitrogen is stored in deep reservoirs, like in the mantle, in the crust or on the oceans, on Venus such processes do not occur and almost all of it remains in the atmosphere.

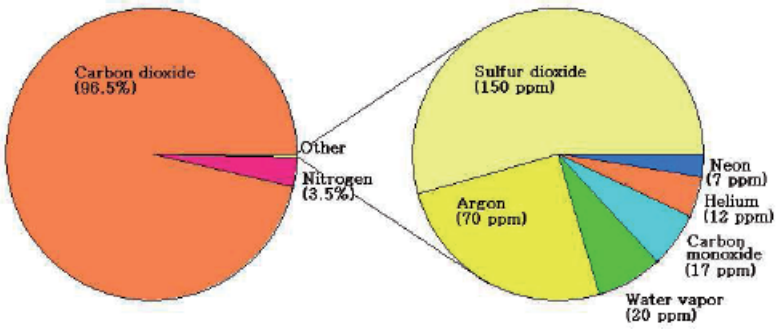

Figure 2.5: Relative composition of Venus's atmosphere with relative abundances of minor species at the right side. (Figure: NASA website).

In addition to the composition, we also have to talk about the physical parameters such as pressure and temperature. On the surface, the pressure of 92 bars, the extremely high concentration of CO_2 and the presence of reflective clouds of sulfuric acid led the planet to an uncontrolled greenhouse effect that turned it into an arid and torrid desert, with surface temperatures of 735 K that make the existence of liquid water impossible (Bullock et al., 2001). This temperature is high enough to melt lead and this pressure is equivalent to that of a body immersed in the Earth's oceans at a depth of approximately 1 km. It is not yet clear whether the surface temperature was ever low enough for water to condense, even under hypothetical conditions of reduced solar illumination in the early Solar System. This makes Venus the prime candidate for study when looking for a comparison with Earth. The surface temperature is about 3 times above the calculated subsolar temperature, again a result of the powerful greenhouse effect (Pedro Machado, 2014).

The solar constant of Venus is almost twice that of Earth, and the effective temperature is 232 K. However, because of the dense and extensive layer of highly reflective clouds that covers the entire planet and leads to a high albedo (reflection coefficient) of approximately 75% (2.5 times the Earth's albedo), Venus absorbs less sunlight than Earth, since not even 10% of the incident solar flux manages to penetrate and travel through the entire atmosphere until reaching the surface. Despite this and as a direct consequence of a strong greenhouse effect, the surface of Venus is the hottest in the solar system, and its temperature is approximately 500 K higher than that observed at the top of the clouds (Pollack et al., 1980). A large thermal inertia is implied due to the massive and dense atmosphere, which leads to a nearly uniform surface temperature (isothermal surface) with latitude and between the day and night hemispheres (Pedro Machado, 2014).

2.3 Atmospheres of telluric planets

Telluric planets are smaller, rockier and therefore denser planets, usually with metallic cores, silicate mantle, and the presence of heavier elements (Si, Mg, Fe, C, O). These planets lose their original hydrogen/helium envelope in the early years because it escapes from the planet because of its lower mass, and therefore lower escape velocity, or even by stellar activity. In our Solar System the telluric planets are the four closest to the Sun (Mercury, Venus, Earth, and Mars); however, some icy moons from gas giant planets like Titan and Io can behave like telluric planets, and also our own Moon has a deniable

resemblance to Mercury (European Space Agency, 2020). Then, they may or may not retain a secondary atmosphere if they have enough mass to maintain it. These secondary atmospheres can be created by a complex combination of processes (Pedro Machado, 2014):

- accretion of solids (like planetesimals) and gases;
- orbital migrations;
- collisions and impacts with external objects (cometary bombardment or/and asteroid material);
- mass loss by evaporation/sublimation of deposited materials in the surface or interior
- atmospheric erosion;
- geophysical evolution;
- outgassing.

The interaction between these processes and the environment in which they are located, including the type of host star and its distance from it, can produce a wide and varied range of results (European Space Agency, 2020). The temporal evolution of the atmospheres of terrestrial planets depends on interactions between the surface and the atmosphere itself. These interactions can occur through chemical reactions between the lower atmosphere and minerals present in surface rocks or through geological processes between the mantle, crust, and surface. These processes can have consequences for the composition of the atmosphere, the greenhouse effect, and the radiative transfer profile because the release of volatiles from the planet's interior into the atmosphere is driven by geothermal energy (Pedro Machado, 2014) (Bullock et al., 2001).

The gas molecules present in those atmospheres are part of the same material that gave rise to the solar system. The formation of these gas layers around the solid globes was probably a consequence of accretion that then suffered a continuous degassing of volatiles, resulting from an intense outgassing of the mantle, amplified by the heating caused by the differentiation process of the core (Bullock et al., 2001). Since they came from the same solar nebula, it was expected that the atmospheres' composition of our terrestrial planets would be similar, as were the primary atmospheres, however, the different evolution of these planets led to significant changes between the secondary ones. With sufficient mass, a planet will have a hot and active inner core due to both the process of planetary formation and the radioactive decay of unstable elements in its interior. This heat releases gases that can migrate from the interior to the surface, and then to the atmosphere. However, because of their high kinetic energy, atoms and light molecules can escape into space, but it is possible that other mechanisms could retain these molecules in the structure of the planet in a solid or liquid phase (Pedro Machado, 2014) (Bougher et al., 1997).

In the Solar System, we have four celestial bodies capable of retaining and maintaining a terrestrial-type atmosphere (see Figure 2.6). One of them is not even a planet but Saturn's biggest moon, Titan. We also have bodies with an undeveloped atmosphere with only a thin and tenuous layer (exosphere) that is not in hydrostatic equilibrium; this is the case for Mercury and Io. For terrestrial-type atmospheres, the different layers of gas must be in hydrostatic balance, which is characterized by vertical stabilization, where each horizontal layer is supported by the pressure differential between adjacent layers (Pedro Machado, 2014).

Between those four bodies with terrestrial-type atmospheres, we have some characterized by slow rotational motion (Venus and Titan, despite having a super rotating atmosphere) and others by fast rotational motion (Earth and Mars). In the last case, the Coriolis force and the pressure gradient dominate in

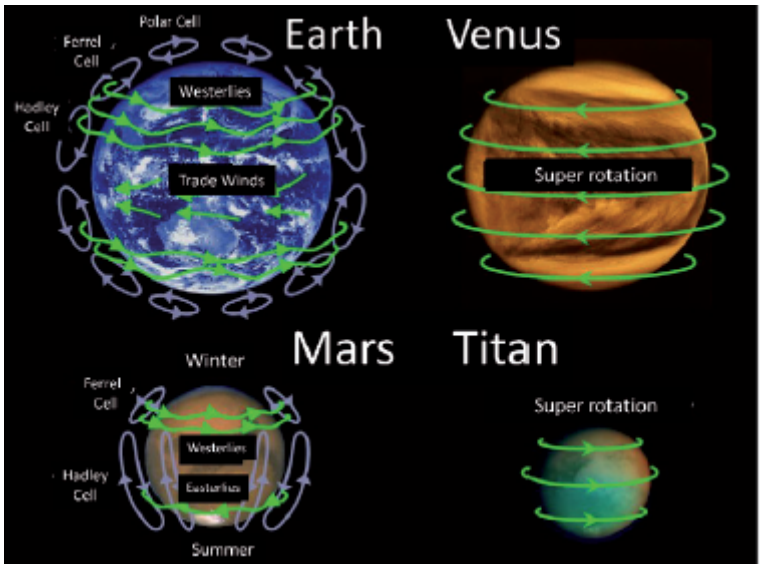

Figure 2.6: The atmospheric global circulation of Solar System's terrestrial-type planets. From Pedro Machado (2014).

the momentum equation, the centrifugal force is neglected, and the wind blows along the isobars and is perpendicular to the pressure gradient; this is called the geostrophic balance (Agustín Sánchez-Lavega, 2010). In the first case, we neglect the Coriolis force and not the centrifugal one, which balances the pressure gradient, generating steady horizontal wind flows almost parallel to the equator and strong zonal winds and jets prevailing in the stratosphere; this is called the cyclostrophic balance (Pedro Machado, 2014).

Venus is a planet dominated by CO_2 (like Mars); its high atmospheric abundance contributes decisively to the enormous greenhouse effect, adding around 450 K to its sub-solar temperature (by comparison, the greenhouse effects of Earth, Mars and Titan only add around 35 K, 7 K and 12 K to their respective sub-solar temperatures). As a consequence, the atmospheric profile of Venus (see Figure 2.7) shows a higher surface temperature and pressure than the other telluric planets, the absence of temperature inversion in the ozonosphere, as in Earth, and the temperature difference between the day and night thermospheres; the thermospheric temperature on the night side decreases with altitude, while on the day side increases, due to the slow rotation of Venus (Pedro Machado, 2014) (Schubert et al., 1980).

We have already addressed the possible common starting point in the planetary disc followed by distinct planetary evolutions. The current time differences among the telluric atmospheres of the solar system, with attention to Earth-Venus comparison, are as follows: the solar constant (or the flux) of Venus, which is twice that of Earth; the faster rotation speed of Earth, which emphasizes geostrophic equilibrium (as on Mars) and contrasts with the cyclostrophic equilibrium on slower planets (Venus and Titan); the presence of an internal magnetic field and magnetosphere on Earth, in contrast to the weak induced magnetic field of Venus due to the interaction between the solar wind and the upper atmosphere; the 23° obliquity of Earth, in contrast to the inverted axis of Venus that is nearly normal to the ellipse; the distinct compositions of the atmospheres of Venus and Earth; the greater density and surface pressure on Venus; the faster winds on Venus (zonal superrotation); the presence of water vapor and oceans on Earth, in contrast to the near absence of water on Venus; the distinct temperature profiles; the runaway greenhouse effect on Venus, in contrast to a much weaker one on Earth; the condensable water vapor on Earth, contrasting with sulfuric acid on Venus, carbon dioxide plus water on Mars, and methane plus ethane on Titan; the type of volcanism and plate tectonics on Earth, in contrast to the single plate on Venus; and finally, the presence of a satellite (the Moon) that influences and stabilizes Earth's rotation,

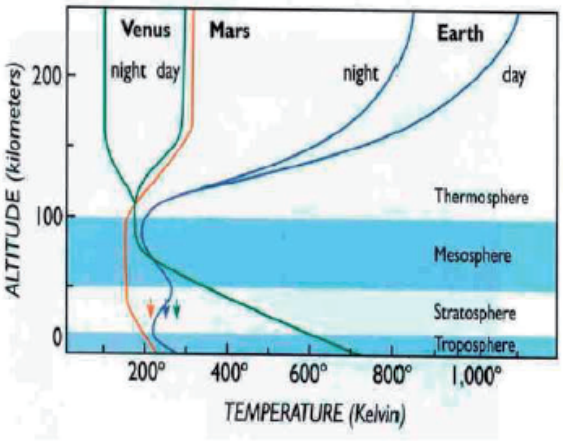

(a)

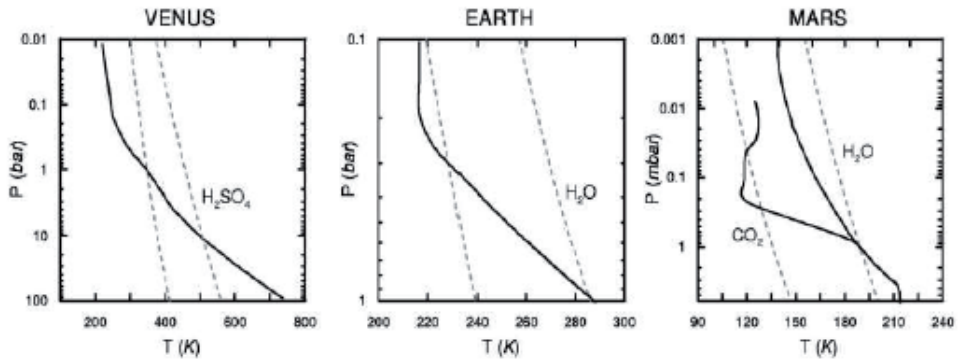

(b)

Figure 2.7: Averaged thermal profile with altitude (a) and pressure (b) plus condensable species for Venus, Earth and Mars. Figures from Pedro Machado (2014).

in contrast to Venus, which has no satellites (Pedro Machado, 2014).

From the atmospheric composition frame, Venus and Mars are more similar, while Earth stands out by being radically different. However, from a dynamical point of view, because of the nearly equal rotation rate and obliquity, Earth and Mars share more features. In turn, being a slow rotating planet, Venus is dynamically similar to Titan; both bodies neglect the Coriolis contribution, prevailing the cyclostrophic balance (Taylor, 2006). For the meridional circulation frame, on Venus, there is only one Hadley cell (a cell that carries air from lower latitudes to higher latitudes), extending from the equator to the poles (see Figure 2.12), one in each hemisphere; on Earth, which rotates faster, our Hadley cells are restricted to the subtropical latitudes, so that the meridional circulation needs two more cells to reach the polar regions, that is, three per hemisphere (Pedro Machado, 2014). This implies that there are no climatic differences across the surface of Venus and that temperatures are homogeneous across latitudes (one same cell covering all the hemisphere).

2.4 The Venusian Atmosphere

Using the temperature variation profile with altitude, we can divide Venus's atmosphere into three distinct layers. Starting with the lowest layer, we have the troposphere (0-65km). It extends from the surface to the top of the clouds and the temperature decreases with altitude at a rate of $9K/km$ (because

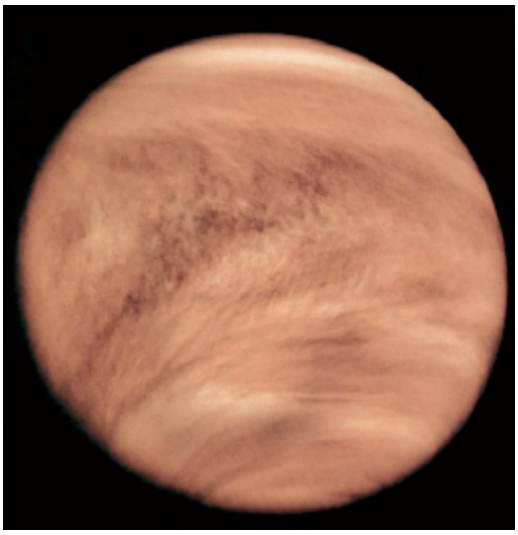

Figure 2.8: Image of Venus taken by the Pioneer Venus's space probe in ultraviolet in 1979. The presence of an Y-shaped cloud pattern is visible. (Image: NASA/JPL website).

it is close to the adiabatic lapse rate, that defines the temperature variation of ascending/descending air without exchanging heat with surrounding, $\Gamma_d = \frac{g}{C_p} = 7.39K/km$, we assume there is no significant convection). Next, is the mesosphere (65-100km). In this layer, the vertical thermal gradient is less evident; however, there is greater horizontal variability as a function of latitude, increasing from the equator to the poles, consistent with the presence of the Hadley cell (Taylor et al., 1979). Finally, we have the thermosphere (100-200km). In this region, there is a balance between the thermal conductivity of the molecules and the incoming UV radiation. However, there is a difference between the day and night hemispheres. Between 100 and 140km, temperatures increase with altitude on the day side and decrease on the night side. Above 140km, the temperatures in both hemispheres remain the same (Pedro Machado, 2014).

The clouds absorb around 92% of the incident solar flux that is not reflected back to space (due to the high albedo), and just the remaining 8% will eventually reach the surface (a lot different from Earth). About half of that absorbed solar radiation is due to unidentified UV absorbers found primarily in the cloud layer (Pedro Machado, 2014).

Venus's atmospheric dynamics are essentially governed by solar thermal heating and its very slow rotation rate (a year shorter than a day), making them quite different from Earth's. It is the balance of pressure gradient forces, the precise equatorward component of the centripetal force (cyclostrophic equilibrium), that dictates the system of horizontal winds parallel to the equator (the Zonal Winds), unlike what occurs in the geostrophic regime. Although Venus is a planet completely overloaded with CO_2, its atmospheric balance is currently highly dependent on SO_2 concentration, it is safe to say that minor components are important in atmospheric coupling (Pedro Machado, 2014) (Bullock et al., 2001).

The thick layer of clouds that completely covers the surface results from photolysis and recombination processes of H_2O and SO_2 (see Figure 2.9) that react with CO_2 following a reaction chain that generates droplets of sulfuric acid, with high reflectivity (Pedro Machado, 2014):

$$CO_2 + SO_2 + h\nu \longrightarrow CO + SO_3 \tag{2.1}$$

$$SO_3 + H_2O \longrightarrow H_2SO_4 \tag{2.2}$$

Therefore, these clouds consist essentially of sulphuric acid droplets in a 85% water solution. Over time, both SO_2 and CO tend to sink in clouds towards the surface. The cloud layer extends from 48km to 70km altitude, with faint hazes above (up to 90km) and below (from 30km) the main deck (Esposito et al., 1983). The clouds are not homogeneous since there are aerosol particles of different sizes. In the upper layer (57-70km) particles have an average radius of 0.3μm and a total optical depth of 7 at 0.63μm. In the intermediate region (51-56km), particle sizes range from 1 to 1.4μm, with an optical depth, at the same wavelength, of 9. Finally, in the lower zone (48-50km), the optical depth is almost 10, due to 3.65μm particles (Pedro Machado, 2014) (Knollenberg et al., 1980).

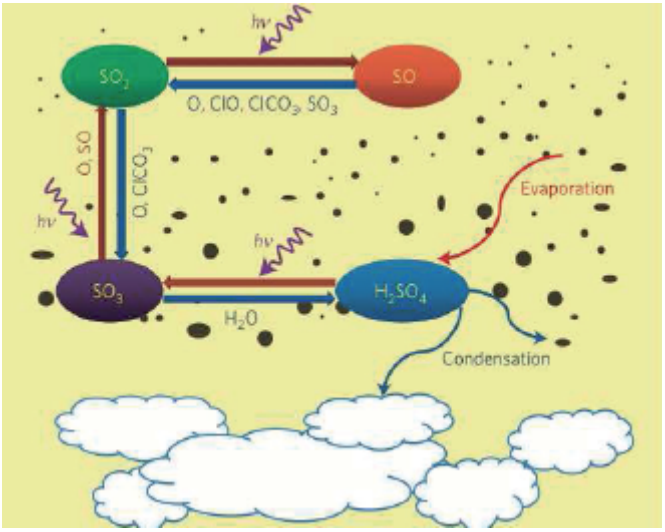

Figure 2.9: The cycle of SO_2 in Venus's atmosphere and respective radiative interactions. From Pedro Machado (2014).

In the polar region (high latitudes), we can see a huge vortex, similar to the hurricanes on Earth but four times larger. In the equator region (low latitudes), the mottled cloud pattern shows signs of convection and turbulence. In medium latitudes ($\approx 50^o$), we see bands of nearly zonal flow, the retrograde zonal wind (constant with latitude), which fades away, decreasing in velocity toward the pole (Markiewicz, Titov, Limaye, et al., 2007); this latitude region could be the poleward branch of the Hadley cell in the meridional circulation. Here, it is possible to observe the mid-latitude jet, where the wind can increase to $20m/s$, although it is not always visible (Titov et al., 2008). In 2007, the presence of lightning in Venus's atmosphere was confirmed by Venus Express's magnetometer. These electrical discharges are important because they can be an energy source for high-altitude atmospheric chemistry (Pedro Machado, 2014).

Photolysis is the primary and one of the few processes responsible for the loss of atmospheric CO_2 on Venus. H_2O is also lost by the same process. SO_2 is lost in the reactive process of sulfuric acid formation and some surface-atmosphere interactions deposit it on the ground,. Thus, volcanism is the main source of replenishment of these molecules, especially CO_2. During an episode of large-scale volcanism, their amounts increase, followed by a period of gradual reduction until the next episode. In the early history of Venus, atmospheric water vapor was responsible for the greenhouse effect. Later, the water molecule went through a process of dissociation in the upper atmosphere, where its oxygen was being captured to form sulfur compounds, and the hydrogen reached escape velocity and escaped the planet. This resulted in a massive loss of water, and so the greenhouse effect started to be driven by CO_2 (Pedro Machado, 2014).

Although they exist in smaller quantities in the atmosphere, SO_2 and H_2O play a significant role in the thickness of the cloud layer. Drastic changes in volcanic activity, surface-atmosphere reactions, or

atmospheric escape could disrupt the balance of these species. If the atmospheric replenishment sources of SO_2 and H_2O were compromised and their quantities decreased, the cloud layer would become much thinner and could even dissipate completely in a few million years (Bullock et al., 2001). It is possible that Venus has had clear skies in the past and may experience the same again in the future. The albedo would also become much lower due to the reduced reflectivity of the clouds, affecting the atmospheric radiative transfer process and the surface temperature. Therefore, a decrease in the release of SO_2 would condemn the planet to even greater global warming and the greenhouse effect. The constant loss of atmospheric water through exospheric escape could make the formation of sulfuric acid in clouds much more difficult and rare, affecting the albedo again and also leading to an increase in temperature. However, since water vapor is a greenhouse gas, its decrease implies a reduction in the overall effectiveness of the greenhouse effect. Despite that, this side effect would be smaller because the greenhouse effect is currently essentially controlled by carbon dioxide. In the opposite scenario, an increase in the release of SO_2 would interfere with geological processes at the crust level (Bullock et al., 2001). Currently, because of the high temperature, carbon dioxide does not react with the surface, as it exists in a supercritical state. A hypothetical increase in the amount of volcanic SO_2 would cool the surface temperature to a point where carbon dioxide could react with minerals in the soil and be buried as carbonated rocks (as on Earth). This would weaken the greenhouse effect and further cool the planet, potentially leading to a new planetary equilibrium with much lower surface pressures and temperatures (Pedro Machado, 2014).

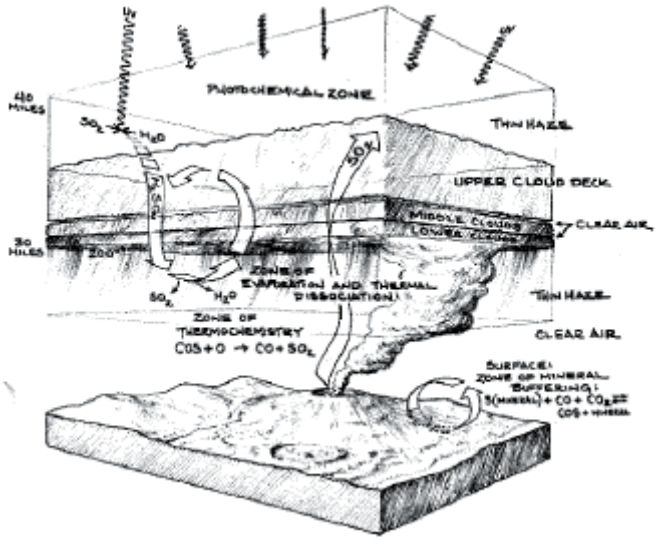

Figure 2.10: Illustration of Venus's atmospheric structures and interactions. From Pedro Machado (2014).

2.4.1 Global atmospheric circulation

Many efforts have been made over the years by the scientific community to fully understand the global atmospheric circulation of Venus; however, there is still no theory that explains it exactly, and the way in which Venus reached and maintained this state of super-rotation of the atmosphere is still controversial. Some measurements of zonal winds have already been made using the cloud tracking technique at ultraviolet, visible, and infrared wavelengths (Markiewicz, Titov, Ignatiev, et al., 2007) (A. Sánchez-Lavega et al., 2008); this is useful because we will later make a comparison between those results and those of the ground-based method that we will use in this work (Pedro Machado, 2014).

How the super-rotation process is driven and maintained over time is still an open question. The huge

contrast between the high wind velocities of the atmosphere and the slow rotating planet is not yet well explained. The rotation depends only on latitude; if we choose one single latitudinal circle around the globe, the zonal wind velocity is constant, so it does not depend on longitude. The first evidence of a fast retrograde westward (clockwise) motion was found in the ultraviolet wavelength range; where a large scale Y shaped feature, defined as a planetary global scale wave, circling the planet in four days, could be seen. The current long rotational period can also be due to the gravitational tidal force of the Sun (slowing down the rotation) and the atmospheric torque (Pedro Machado, 2014) (Bougher et al., 1997).

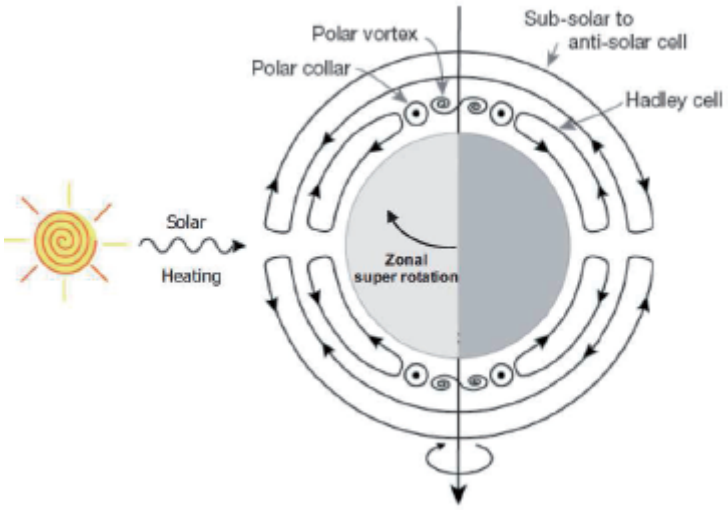

Figure 2.11: Illustration of Venus's global atmospheric circulation. From Pedro Machado (2014).

In the lower and middle atmospheres and at low latitudes, circulation is controlled by convection. In mid-latitudes, we have the retrograde zonal wind (RZW), and a jet stream can sometimes be detected, although it is highly unstable. In the polar region, near the axis, a large binary vortex (also highly variable) was found, covering several square kilometers and rotating with a period of just a few Earth days (Pedro Machado, 2014).

Three main atmospheric motions characterize the global dynamics of Venus's atmosphere. In the mesosphere, most predominantly at mid-latitudes, we have the crucial and mysterious super-rotational RZW, which flows in bands parallel to the equator and will be further measured and studied as the objective of this work. Higher in the thermosphere, we have the sub-solar to anti-solar (SS-AS) circulation, which transports the overheated air from the daytime to the nighttime hemisphere. It should be noted that, because of the long rotation period, the hemisphere facing the Sun (sub-solar) already has an excess of radiation received compared to the opposite (anti-solar) hemisphere, which has a deficit. The third motion is the meridional circulation, which transports the excess heat from low-latitude regions toward the poles, cooler high-latitude regions. As already mentioned, this circulation is carried out by a single Hadley cell in each hemisphere: the warmed equatorial air rises, then is transported by the upper limb of the cell to high latitudes, where it cools, sinks, and returns to low latitudes along the lower limb of the cell (Pedro Machado, 2014) (Limaye, 1985).

The altitude band from 65 to 120km in the atmosphere acts as a transition region between the RZW circulation of the lower atmosphere and the SS-AS circulation of the upper thermosphere. The co-existence of these two types of circulation can be demonstrated through thermal profiles made in this region of the atmosphere, with zonal winds decreasing with altitude and thermospheric winds increasing (Bougher et al., 1997) (Lellouch et al., 1997) (Hueso et al., 2012). In the lower mesosphere (65 to

85km), observations of the Fraunhofer solar lines in the visible spectrum were made, and Doppler shifts were detected, allowing the only cloud-top Doppler wind measurements in recent years (Widemann, Lellouch, and Campargue, 2007) (Widemann, Lellouch, and Donati, 2008) (Pedro Machado et al., 2012) (P. Machado, Widemann, J. Peralta, et al., 2014) (P. Machado, Widemann, Peralta, et al., 2017) (Gonçalves et al., 2020). This region is important because it helps constrain the global atmospheric circulation.

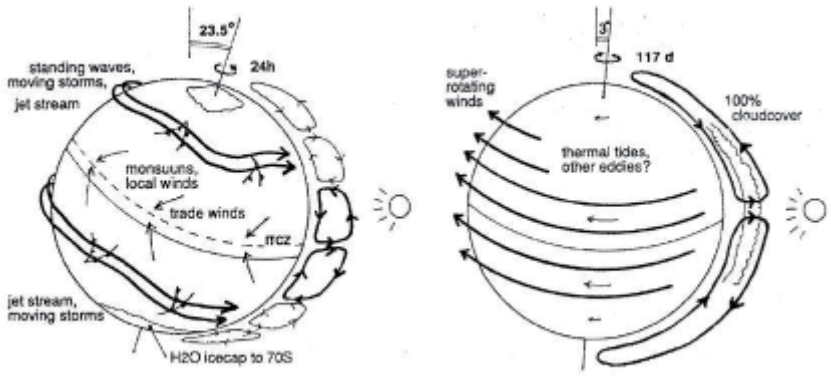

Figure 2.12: Planetary atmosphere motion for Earth (left) and Venus (right) at large-scale: different types of circulation patterns are visible in relation to latitude, altitude and local time. From Pedro Machado (2014).

At the cloud tops, the winds have velocities of a hundred m/s, however, near the surface, the winds are very slow, with velocities on the order of just some m/s, this is due to the general independence of temperature in relation to latitude, since the planet has low obliquity, so there are no seasons (Crisp et al., 1990), and only one Hadley cell per hemisphere, homogeneous temperature. The range of altitudes where the cloud layer resides has been particularly studied, with a greater focus on the top of these clouds, since observation is easier and velocities can be obtained using various techniques: cloud tracking, Doppler velocimetry, and thermal winds. In all these techniques, the constant state of superrotation of the atmosphere can be identified, throughout the entire cloud layer, with the zonal wind circling the planet in about 4.4 Earth days ($\approx 100m/s$), approximately 60 times faster than the planetary body itself (Pedro Machado, 2014).

There are three theories that attempt to explain the possible causes of the super-rotation of Venus's atmosphere: the SS-AS circulation mechanism (see Figure 2.11), currently the one with the fewest supporters; the thermal tide mechanism, planetary-scale atmospheric waves produced by solar heating; and the meridional circulation mechanism made by the Hadley cell. The second theory is possibly the most likely, but the hypothesis that combines the latter two theories is quite plausible. Thermal tides function as two forces: one at the cloud tops pointing upward and the other at the cloud bottom pointing downward. Due to the conservation of momentum, a force is created that pulls the cloud deck forward and initiates rotation. However, the wave would have to oscillate upward and downward, creating negative critical levels where they don't exist. Therefore, it is necessary to study the structure of the meridional and vertical circulation (thermal tides). In recent years, several models of global atmospheric circulation have been performed to reproduce super-rotation and verify these theories. Since the atmosphere and the globe rotate in the same westward direction (clockwise), if for some reason the atmosphere gained angular momentum (accelerate), the globe would have to lose an equivalent amount, and vice versa, according to the conservation angular momentum of the atmosphere-globe system (Takagi, 2025).

2.5 History of Venus exploration

Since the beginning of modern space exploration, more than 30 spacecraft have been sent to Venus, it was our first target for planetary studies and space exploration. The first close contact was made with the space probe *Mariner 2* in 1962; although it was the first, it was already able to measure surface temperatures with its magnetometer (Sonett, 1963). From the same program, *Mariner 10* was able to collect image data with a 30*km*/pixel resolution, in 1974, during its closest approach to the planet (NASA, n.d.[b]).

Another very important program was the *Venera* program from 1961 to 1984. The first try, *Venera 1*, went rogue after losing contact with ground control. However, further missions were quite successful. *Venera 4* (1967), for example, collected the first atmospheric data and sent them back to Earth. *Venera 5* (1983) performed a high-resolution radar mapping of the surface. Most of these last missions also confirmed the presence of a super-rotation atmosphere (Dollfus, 1975). Some of these probes were able to land and stand on the Venusian surface long enough in order to collect data about the surface and atmosphere and transmit back to Earth, under extreme conditions. So, this program really contributed to surface mapping, surface imaging, and measurements of atmosphere conditions. The next soviet mission was *Vega*, continuing the work of the previous *Venera* program with the same basic probe and landing design, but this time also using atmospheric balloons, which can survive longer and measure pressure, temperature, and even wind velocity (Pedro Machado, 2014) (Blamont, 2008).

The Pioneer Venus mission, with an orbiter and multiprobe, began in 1978. Its highly elliptical orbit allowed for mapping of the different layers of the atmosphere and the surface. The descent probes were used to study the composition of the atmosphere and were important for the construction of atmospheric models. This project was the first to study and measure the weak induced magnetic field of Venus, the first to measure the mesospheric winds through the observation of the UV signatures of the cloud tops, the first to discover the double vortex in the north polar region and also for measurements of the constituents of the atmosphere (Pedro Machado, 2014) (Oyama et al., 1980).

In 1992, the Magellan probe mapped nearly the entire surface of the planet using radar. This mission also collected data on Venus's gravity, surface topography, and electrical characteristics. At the end of the mission in 1994, the probe initiated a collision maneuver with Venus to obtain atmospheric data during descent (Pedro Machado, 2014) (Saunders et al., 1992).

After a more than 20-year hiatus in space exploration of Venus, the European Space Agency (ESA) launched Venus Express in 2005. The probe's objectives were to study and monitor Venus's global atmospheric circulation, chemical reactions in the clouds and between the surface and atmosphere, atmospheric escape, volcanism, and the greenhouse effect. Its highly eccentric polar orbit allows for local and detailed spectroscopic observations with high spatial resolution and plasma measurements at perihelion, due to low orbital altitude, and general monitoring on a global scale at aphelion, such as the polar vortex and atmospheric dynamics (Hueso et al., 2012). The probe was equipped with a magnetometer, a monitoring camera (VMC), a visible/infrared spectrometer (VIRTIS), a radio band Fourier spectrometer (PFS), a near-infrared spectrometer and ultraviolet detector (SPICAV), and a plasma plus neutral particles detector (Pedro Machado, 2014).

Using VIRTIS and VMC, it was possible to calculate wind speeds using the cloud tracking method and then compare them with thermal winds derived from VIRTIS observations (Piccialli et al., 2008). This comparison verified the cyclostrophic nature of global atmospheric circulation in the Venusian mesosphere. Venus Express observations provided quantitative measurements of the RZW, revealed the presence of electrical storms in the clouds (Russell et al., 2007), confirmed the existence of atmospheric

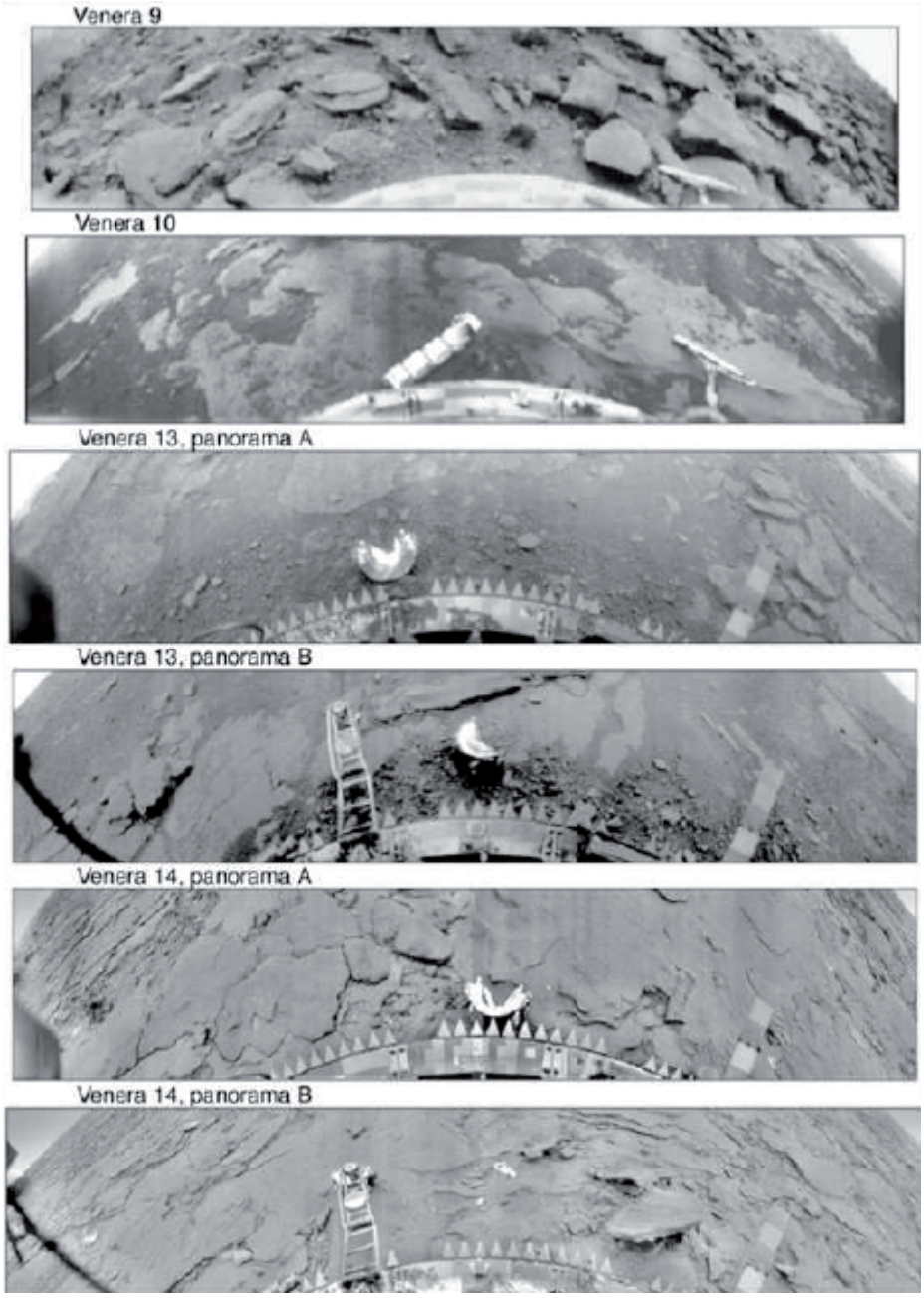

Figure 2.13: Various Venera program landings in the Venusian surface throughout different missions. (Image: Russian Academy of sciences).

vortices in the polar regions, studied with high spatial resolution and long temporal coverage the 4-day super-rotation of the mesosphere at low latitudes, verified the enormous variability of the atmospheric SO_2 concentration, and measured a 2:1 ratio between the atmospheric escape fluxes of hydrogen and oxygen (Pedro Machado, 2014). However, despite its great achievements, the Venus Express mission had to come to an end, with the final contact made at the end of 2014, and with the probe losing its orbit and most likely burning up in Venus's atmosphere (European Space Agency, 2014).

Fortunately for Venus admirers, a year later in 2015, a new spacecraft, this time developed by the Japanese agency JAXA, entered Venus's orbit, an equatorial one, complementary to the Venus Express, after having failed the maneuver on its first attempt five years earlier in the year it was launched in 2012 (NASA, n.d.[a]). This spacecraft belonged to the Akatsuki mission, and its main objective was to

study the dynamics of Venus's atmosphere in three dimensions, with an emphasis on its superrotation. Furthermore, the probe was able to detect stationary gravitational waves on a planetary scale; perform thermal mapping; study the morphology of clouds with possible electrical storms; and monitor long-duration wave patterns. Unfortunately, after nine years in orbit, an anomaly in the spacecraft's control system caused communications to be lost. Subsequent attempts to connect were made, but without success (Spacecraft and Vehicles, 2025).

The next major project in space-based exploration of Venus is scheduled for 2031 with the launch of Envision, ESA's fifth M-class mission in partnership with NASA, within the Cosmic Vision program. Envision will be the first spacecraft to study Venus from its core to the outer layers of the atmosphere, investigating the interactions between them and their evolution over time. It will be the most comprehensive examination of Venus to date, encompassing geology and geochemistry with atmospheric science (European Space Agency, 2025).

Since we will have at least another six years without space-based observations of Venus, it is important to turn now to ground-based observations, as for now, this is the only means of observation we have. Therefore, for this purpose, we will use the Doppler Velocimetry technique using instruments such as UVES on the VLT. This technique will be very important for studying the dynamics of Venus's atmosphere until the next space probe is ready, as it allows us to directly measure with high precision the velocities of zonal and meridional winds at the cloud tops; we will go into more detail in the next chapter (Pedro Machado et al., 2012). Venus is a very important planet for planetary science in general. However, it is an even more special case for us due to the inevitable comparison with Earth, in order to better anticipate and predict the evolution of Earth's atmosphere and to better understand the atmospheres of exoplanets (Pedro Machado, 2014).

Chapter 3

Method

3.1 UVES - Ultraviolet-Visual Echelle Spectrograph

Figure 3.1: ESO's VLT facility in Paranal, in Chile's Atacama desert, where UVES is located. (Image: ESO's website).

UVES is one of the four telescopes in the VLT (Very Large Telescope), located at Cerro Paranal in the desert of Atacama, Chile (see Figure 3.1). It is the second Unit Telescope, or Kueyen, which means "moon" in the native language of the ancient people of Chile. The VLT is part of the European Southern Observatory (ESO) and UVES is a cross-dispersed echelle spectrograph designed to operate from $300nm$ to nearly $1100nm$, it is the perfect combination between spectral resolution and wavelength coverage. It has a very high resolving power of 40,000 when using a 1 arcsec slit (D'Odorico et al., 2000), its light beam is split into two arms, the UV-Blue arm ($300-500nm$) and the Visual-Red arm ($420-1100nm$); these arms can operate individually or simultaneously with the help of a dichroic beam splitter; that reflects only the light below a certain wavelength and not the longer ones. When using a narrower slit or an image slicer that converts 2D images into 1D slits so that the light that normally falls outside the slit is fed to the spectrograph, the two-pixel resolution is 80,000 for the blue arm and 110,000 for the red arm. The instrument has a calibration accuracy for the wavelength scale of at least $50m/s$; however, an iodine cell can be inputted, superimposing many molecular absorption lines on the observed spectrum, enabling accurate wavelength calibration in the $500-600nm$ range, for observations that require a higher accuracy (European Southern Observatory, 2007).

Echelle spectrographs are indispensable tools on large telescopes, as high-resolution spectroscopy greatly benefits from a large light-collection area. UVES is capable of studying the dynamics of gas and

stars in the galactic center, observing the mass distribution in star clusters, evaluating the composition and physical conditions of the interstellar and intergalactic medium (especially gas near high redshift QSOs), monitoring seismology and stellar oscillations through radial velocity studies with high precision and long observation periods (Pedro Machado, 2014).

	Blue Arm	Red Arm
Wavelength range	300–500 nm	420–1100 nm
Resolving power-slit product nm/pixel	41,400 0.0019 nm at 450 nm	38,700 0.0025 nm at 600 nm
Max. Resolving power (2-pixel sampling)	∼80,000	∼110,000
Throughput at blaze (TEL+UVES, no slit, no atm.)	12% at 400 nm	14% at 600 nm
Limiting magnitude (90m exp. time, S/N=10, 0.7 arcsec slit,seeing 0.7)	18 R=58,000 at 360 nm	19.5 R=62,000 at 600 nm
CCDs	2048 × 4096 (windowed to 2048 × 3000)	two 2048 × 4096 (mosaic of different types)
Pixel (15μm) scale disp. dir. (varying along order) along slit (dep. on cross-disp.)	 0.215″ ± 20% 0.25”(CD1 and CD2)	 0.155″ ± 20% 0.18”(CD3),0.17 (CD4)
Echelle (R4 mosaic)	41.59 g/mm	31.6 g/mm
Cross dispersers Blaze wavelength Blaze wavelength	CD1: 1000 g/mm 430 nm CD2: 660 g/mm 460 nm	CD3: 600 g/mm 560 nm CD4: 312 g/mm 770 nm
Typ. wavel. cov. CD1 and CD3 (CD2 and CD4 in parenthesis)	85 (126) nm in 33 (31) orders	200 (403) nm in 37 (33) orders
Min. order separation (standard setup)	10 arcsec (40 pixels)	9 arcsec (51 pixels)

Figure 3.2: UVES characteristics and observing capabilities. From UVES manual, European Southern Observatory (2007).

Between spectral orders' centers, there is a separation of 10 arcsec in the blue arm and 9 arcsec at the red arm that is produced by the cross-dispersers, two in each arm, operating as reflectors of first order for all UVES wavelength range (Dekker et al., 2000); making spectroscopy possible for large objects like Venus. Electronic 2D-array detectors that convert photons into electrons (Charge-Coupled Devices) are equipped in both arms of the telescope: two in the red arm and one in the blue (Dorn et al., 2000). The CCD in the blue arm is a 2000px/4000px chip, EEV type with 15μm per pixel. The red arm has a CCD of the same type and another of the MIT type also with the 2000px/4000px size. The EEV CCD is more effective in the ultraviolet range, while the MIT is more effective in the NIR. Other devices equipped in the instrument are: calibration lamps; the iodine cell (I_2); a Thorium-Argon (Th-Ar) lamp used for wavelength calibration in precise radial velocity studies; the image slicers; a derotator to obtain a perfect slit alignment between the planetary rotation axis and the telescope field; a depolarizer; and an ADC to correct the atmospheric dispersion and compensate for differential refraction in the terrestrial atmosphere (Pedro Machado, 2014).

An important parameter is how much spectral range can a single exposure cover. For these observa-

tions, it is important to use a large diameter class telescope, such as the VLT, since the signal-to-noise ratio (S/N) increases with the square diameter of the telescope. The effectiveness of the spectroscope is a function of the spectral resolution (R); the flux (S), which depends on the collecting area (the diameter); and the central wavelength of the observation(λ) (D'Odorico et al., 2000).

$$1/\sigma_{RV} \propto \sqrt{S\lambda R} \tag{3.1}$$

So, if we want to reduce the error of the radial velocity measurements (σ_{RV}), keeping the same resolution and wavelength, we need to increase the diameter of the telescope. If we want to increase the spectral resolution, we need to use a larger echelle, which is already assured by UVES and its custom-made echelle of high quality, or a thinner slit (the wavelength resolution also depends on this parameter). The slit unit is composed of two reflecting aluminum blades, which allow adjusting the opening of the spectroscopic slit between 0.15 and 20 arcsec. These blades can be seen through the slit viewer camera, which gives us an image of the target field (see Figure 3.3 (a)), this way verifying the acquisition field and tracking. UVES is a top instrument within high-precision spectrographs due to the wide wavelength range covered, the high collecting power of the VLT, and the small pixel size of just $15\mu m$ (Pedro Machado, 2014) (D'Odorico et al., 2000).

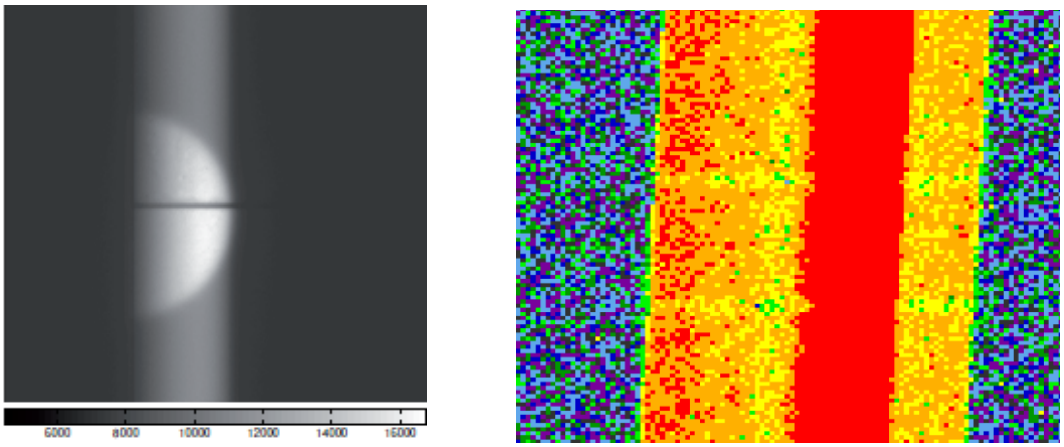

(a) (b)

Figure 3.3: Image from the UVES slit viewer camera, showing the spectroscopic slit on the disc of Venus (a), from Pedro Machado (2014). View of a portion of a spectral order obtained in the DS9 software (b). The horizontal direction corresponds to the spatial variation and the vertical direction to the spectral variation. We can see the different portions of the slit (in pixels) that take different parts of the disc: the red band corresponds to the dayside, the mixture of yellow, orange and red pixels corresponds to the nightside and outside the disc, the mixture of green and blue pixels corresponds to the inactive window of the slit.

The wavelength calibration technique based on Thorium-Argon exposures is the best one because it does not overload the radiation from the target source (unlike the iodine cell) and a wide range of wavelengths are covered (from 380 to 690nm); both spectra, from the target and from the lamp, follow the same path on the detector, so if some instrumental drift is to occur during the measurement process, the two spectra will be affected equally; the lamp also has a high optical stability, requiring less exposure time, easier data reduction, and a better S/N ratio. When measuring radial velocities, we are limited to the line-of-sight component of the velocity, the method is not sensitive to inclinations of orbit nor to the transverse component of the velocity in relation to our line-of-sight from Earth's surface. So, the measurements made must be deprojected from our line of sight to get the real values in the target frame; to do that, all measurements are transformed by the geometric factor to correct them from their intrinsic projection (Pedro Machado, 2014).

	Blue, EEV	Red Mosaic
Quantum efficiency	49% at 320 nm 56% at 350 nm 82% at 400 nm 88% at 500 nm	89% at 450 nm (EEV) 89% at 600 nm (EEV) 81% at 800 nm (MIT-LL) 46% at 900 nm (MIT-LL)
Number of pixels	2048×3000 (2048×4096, used in windowed readout)	4096×4096 (2048×4096 2×1 mosaic)
Pixel size	15 μm	15 μm
Gain (MIT-LL values in brackets)	low: 1.84 e^-/ADU high: 0.54 e^-/ADU	low: 1.6(1.5) e^-/ADU high: 0.57(0.57) e^-/ADU
Read-out noise fast read-out, low gain (slow read-out, high gain) Ultrafast readout, low gain	4.1 (2.1) e^- rms	EEV 3.4 (2.0) e^- rms MIT 3.8 (3.4) e^- rms EEV 4.6 e^- rms MIT 4.85 e^- rms
Saturation low gain (MIT-LL in brackets)	~65000 ADU	~65000 ADU (~43000 ADU)
Full frame readout (s) at 50 kpix, 2x2 bin at 225 kpix, unbinned at 625 kpix, unbinned	 34 (1-port) 30 (1-port) 6.4 (2-ports)	 45 (2-ports) 40 (2-ports) 10 (4-ports)
Dark current levels	0.4 e^-/pix/h at -120°C	EEV 0.5,MIT 1.1 e^-/pix/h at -120°C
Fringing amplitude at 850nm	-	EEV: up to 40% MIT: up to 20%
CTE	> 0.99993	> 0.99995
Read-out direction	in disp. dir.	in disp. dir.
Prescan, Overscan areas	Pix. 1-50 and 2098-2148	MIT: pix 40-50,2098-3008 EEV: pix 1-50,2098-2148
Flatness	< 15μm peak to peak	< 60μm peak to peak

Figure 3.4: UVES CCDs properties measured. From UVES manual, European Southern Observatory (2007).

3.2 Doppler Velocimetry with UVES

As we have seen, clouds are made of aerosol droplets. As clouds move, these particles are responsible for the Doppler shift, scattering incident solar radiation in all directions, including the observer's one. Because they are in motion, the wave frequency of the received light will have a detectable shift in the absorption or emission spectral lines (depending on the technique). Then, we compare these shifted lines with a chosen reference spectrum to obtain the relative velocities. Next, we measure the variation in wavelength and, through the Doppler effect, obtain the instantaneous and absolute velocity values of the probed area. Generally, the deviations are smaller than the line widths themselves, so it is essential to use an instrument with high spectral resolution. Since the measurements are made only in our line of sight, we must then project these values back onto the reference frame of the Venusian atmosphere from which they were taken, using the projection factor (detailed later). To do this, we need precise navigation of the surveyed points. It is also important to distinguish and identify possible contributions from other

movements, such as meridional or SS-AS circulations (Pedro Machado, 2014).

The main objective of this work is to directly measure wind velocities using visible Fraunhofer lines scattered by particles at the top of Venus's clouds, which corresponds to the maximum speed of zonal super-rotation. The Doppler shift detected from sunlight reaching us after being scattered by the dayside of Venus results from two motions: the motion between the Sun and the particles at the top of the clouds, which scatter the incident radiation in all directions, including ours; and the motion between the observer and those particles, which results from the velocity of the particles in our reference frame, this effect is minimal near Venus's subterrestrial point. The measured Doppler shift is then the sum of these two terms and varies with longitude and latitude. Due to atmospheric motion, light scattered by particles in clouds (at an altitude of about $70km$, where $\tau \approx 1$) undergoes a wavelength shift proportional to the wind velocity. By applying Doppler velocimetry to this radiation, we can study the wind latitudinal profile, its local temporal distribution, and its variability. This technique is an adaptation of the Absolute Astronomical Accelerometry, method proposed by Connes (1985), and has already been successfully applied on Venus in Pedro Machado et al. (2012), also resorting to UVES/VLT observations, providing the first latitudinal wind profile of the planet. Beyond Venus, the method has also been applied to Io (T. Civeit et al., 2005), Titan (Luz et al., 2006), and Saturn.

For these observations, we chose to use only the red arm of UVES, with the *CD*#3 cross-disperser, a below-slit filter SHP700 and a central wavelength of $580nm$. The EEV detector has 23 spectral orders covering the range between 480 and $570nm$, while the MIT detector has only 16 spectral orders cover-itween 590 and $670nm$. Because each CCD covers a different wavelength range, different altitudes are probed by each, since radiation with shorter wavelengths can penetrate the atmosphere further, which can lead to different wind retrievals due to a possible vertical wind shear. To cover a wide range of latitudes and longitudes on the surface of Venus, we used a long-slit configuration with 0.3 arcsec wide and 12 arcsec long. The contrast between the small slit width and the large angular size of Venus allows us to directly determine the latitudinal and longitudinal variation of the zonal winds (Pedro Machado, 2014).

Both the pointing uncertainty of VLT and the offset uncertainty of UVES are equal to $0.1"$, so we assume the overall positioning error of the slit to be:

$$\sigma_{tot} = \sqrt{\sigma^2_{pointing} + \sigma^2_{offset}} = 0.14" \tag{3.2}$$

The active sounding window of the slit corresponds to 65 detector pixels (1 central pixel plus 32 pixels on each side), each pixel is $15\mu m$ in size, corresponding approximately to a 0.182 arcsec pixel scale ($\pm 20\%$) using the red arm *CD*#3 cross-disperser, and is equivalent to 107 km on Venus's surface, so, at disc center, the slit width of 0.3 arcsec corresponds to an angle of approximately 2^o in latitude (Pedro Machado, 2014).

As we can see in the Figure 3.5, the overall detection effectiveness measured for the system (UVES + detectors + mirrors) with the cross-disperser *CD*#3 is approximately 0.14, with an average uncertainty on the individual points of about 5%. For the resolving power, we can see that for slit widths of 0.3 arcsecs in the red arm, $R \approx 110000$.

Using high-resolution spectra from the VLT and the UVES echelle spectrograph, we want to measure the zonal and meridional wind fields in the Venusian dayside mesosphere, characterize the latitudinal profiles, study their variability, and better understand the contribution of large-scale planetary waves on maintaining super-rotation, such as the Y-shaped wave visible in the Venusian atmosphere. Using absolute accelerometry (or Doppler velocimetry) at UVES, we want to measure the Doppler shift in the visible solar spectrum backscattered by Venus's main cloud layer. The latitudinal wind profile also

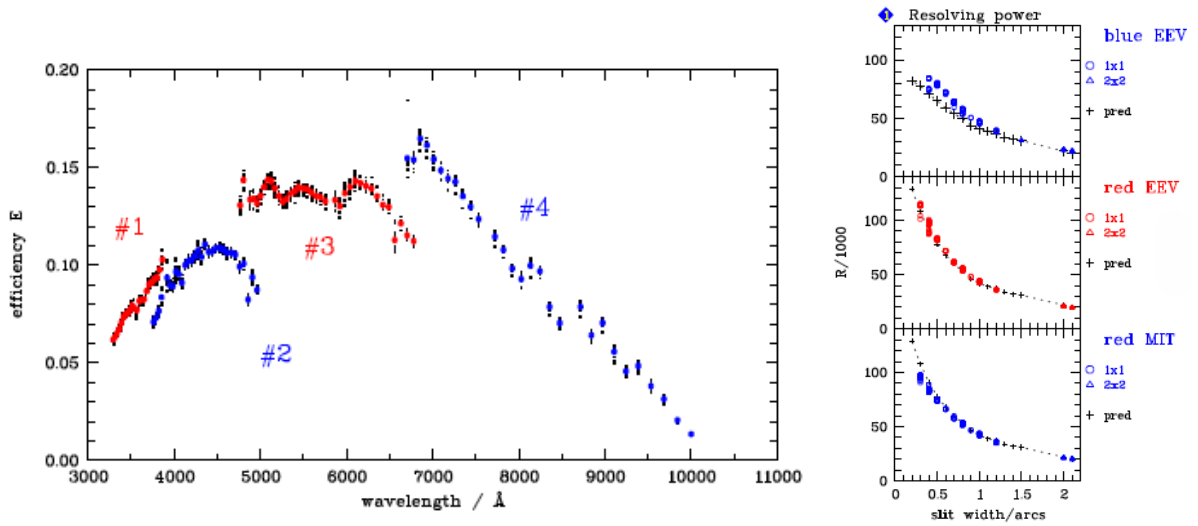

(a) (b)

Figure 3.5: Overall detection effectiveness of UVES + detectors + 3 UT2 mirrors, corrected for the contribution of the atmosphere, for the different cross-dispersers (a). Mean resolving power R (in 1000) as function of the slit width (b). From European Southern Observatory (2007)

provides more information about the coupling of zonal winds and waves, as in the case of the Y-shaped wave, and also allows to evaluate the importance of the meridional angular momentum transport by the Hadley cell. The extremely narrow UVES slit, compared to the size of the disc, allows to perform observations with spatial resolution, both in latitude and longitude. This makes it possible to separate spatially varying wave motions from zonal components, which are constant for a given latitude when the slit is aligned perpendicular to the rotation axis (PP), which is the case (Pedro Machado, 2014).

We also want to compare the results obtained through this method with the values measured by the former Venus Express and Akatsuki mission probes using cloud tracking. The values derived through this technique do not always represent the true wind circulation, as they are perpetually dependent on clouds. Therefore, the measured values may not take into account geological features, such as mountains or ridges, which keep the clouds stationary while the wind and its particles circulate. Also, with this technique it is impossible to directly measure winds above cloud level (Pedro Machado, 2014).

3.2.1 Doppler Shifts

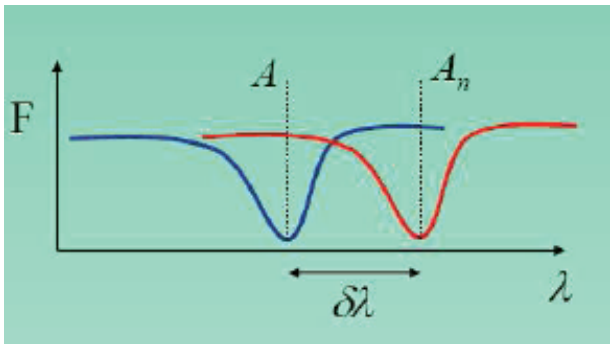

Figure 3.6: Illustration of how to obtain radial velocity using only the shift of one spectral line. From Pedro Machado (2014)

This technique measures the Doppler shifts between absorption lines of spectra obtained simultaneously. This will only get us relative velocities because the absolute Doppler measurements require

a stable velocity reference during acquisition with a grating spectrograph such as UVES (P. Machado, Widemann, Peralta, et al., 2017). First, we assume that the Doppler shifts are obtained based only on one Doppler deviation line (see Figure 3.6), the simplest Doppler shift equation is:

$$\frac{\delta V_n}{c} = \frac{\delta \lambda}{\lambda} \tag{3.3}$$

Where δV_n is the Doppler velocity between the shifted line and reference one, c is the speed of light, λ is the wavelength of the shifted line and $\delta\lambda$ is the wavelength shift between the same two lines. We can also take Taylor's first-order approximation because the shift $I_n - I$ (being I_n the position of the shifted line and I the position of that line in the reference spectrum) is much smaller than the line width, so:

$$I_n - I = \frac{\partial I}{\partial \lambda} \cdot \delta\lambda \tag{3.4}$$

Now, we combine these two equations to get the relative velocity between the shifted and reference lines:

$$\frac{\delta V_n}{c} = \frac{I_n - I}{\lambda \cdot \frac{\partial I}{\partial \lambda}} \tag{3.5}$$

Again, these are relative Doppler shifts between two spectra obtained at the same time and at different slit pixels. So we now express it as function of those pixels:

$$\delta v_i = \frac{c}{\lambda(i)} \cdot \delta\lambda_i = \frac{I(i) - I_o(i)}{\frac{\lambda(i)}{c} \cdot \left(\frac{\partial I_o}{\partial \lambda}\right)_{\lambda=\lambda(i)}} \tag{3.6}$$

Where the index i refers to the pixel of the shifted spectrum and o refers to the reference pixel (slit's central pixel). This is the procedure to retrieve relative velocities by measuring the Doppler shift of only one absorption line. However, to measure Doppler shifts using just one single line fitting, for the values that we want to get (on the order of 100m/s), we would require a spectral resolution (R) of about 10^6, much higher than the UVES's and impossible with current instruments. So we analize the whole spectral range, using the Absolute Astronomical Accelerometry (AAA) technique, rather than line by line, allowing to achieve a theoretical precision of a few m/s. The procedure is applied to a set of absorption lines, the Fraunhofer lines (containing approximately 4400 solar lines), scattered by clouds tops measured simultaneously on the full high-resolution spectrum over the wavelength ranges of the EEV and MIT CCDs. The lines are taken from the planet. A weighted average of the single-line Doppler shifts, using the inverse of each individual line velocity contribution variance as a weighting factor, is then performed (Pedro Machado, 2014):

$$\delta v = \frac{\Sigma(\delta V_i \cdot w_i)}{\Sigma(w_i)} \quad \text{where} \quad w_i = \frac{1}{\sigma^2[\delta v_i]} \tag{3.7}$$

We must assume that the representative noise is only of photonic origin, due to the poissonian nature of photons. Doing so we can calculate each line's relative velocity variance contribution ($\sigma^2[\delta v_i]$) and obtain the radiation's intensity variance directly ($\sigma^2[I] = I$), then the overall uncertainty in the differential velocity determination, that comes mostly from the dispersion relation uncertainty, is:

$$\sigma[\delta v] = \frac{1}{\sqrt{\Sigma(w_i)}} \tag{3.8}$$

The velocity profile is measured as a weighted average of the shifts of the various spectral orders, for

each exposure. The main source of uncertainty is the dispersion of the measurements obtained from the different orders. Resuming, we can determine the Doppler velocity due to line shifts between different points of the disc. However, these Doppler shifts do not yet represent wind velocities as we need to take into account and correct several effects and observational biases (Pedro Machado, 2014).

3.3 Data retrieval and algorithm

Doppler measurement is based on the difference between the shifts measured in each line of the spectrum relative to a reference spectrum, which in this case corresponds to the center of the slit; both spectra are obtained simultaneously. The algorithm measures these Doppler shifts, relative to the reference spectrum, in the line of sight as function of the pixels along the slit, which are then converted to longitude. This reference spectrum always corresponds to the center pixel and has zero shift (Pedro Machado, 2014).

For data analysis and processing, we used an algorithm developed in the Matlab programming language, which had already been previously created, validated, and used in (T. Civeit et al., 2005) (Luz et al., 2006), before being adapted for long-slit measurements of an extensive body such as Venus (Pedro Machado et al., 2012) or Saturn. All data produced are in FITS format. The Flat Fields and Bias files correspond to calibration files, as do the Lamp files for wavelength calibration using the Th-Ar lamp, and the order definition frame files. The data are debiased and flat-fielded using sets of five bias and five flat-field images. The bias files were taken on the same days as the science observations (August 20^{th}, August 29^{th}, and September 3^{rd}, all in 2018), and the flat files were taken on each following day. A master bias and a master flats are then calculated using the median of each set. The wavelength calibration using the integrated Th-Ar lamp allows us to produce a dispersion relation function, which results in a correspondence between each pixel in the echellogramme and its respective wavelength. The two CCDs in the red arm (the EEV and the MIT) are extracted and treated separately, as for the different spectral orders, due to the $20nm$ gap between them. In the extraction process, it is possible to find some pixels damaged in the detector with an unusual response, probably due to the hit of cosmic rays, which are then discarded. In the echelle spectrometer, the long-slit image appears to be curved. This slight curvature produces errors in wavelength calibration, in spectral line shifts, and therefore in measured velocities that cannot be ignored. This problem was also previously solved in Pedro Machado et al. (2012).

The importance of some variables such as noise level, which has a considerable impact in the accuracy of this technique, line density, and line symmetry has been studied resorting to sensitivity tests in which these factors are altered independently. When the SNR or the line density is decreased, the velocity curves obtained are lower than expected, with a higher discrepancy in the spectra farther from the reference one. In line symmetry matter, lines wider on the red side lead to higher velocities, while lines wider on the blue side lead to lower velocities. If not correctly compensated by the ADC prism, the line symmetry can be affected by differential atmospheric refraction, making it a determining factor in the visible wavelength range. (Pedro Machado, 2014)

3.3.1 Observational biases

In each exposure, the measured velocity profile takes into account the weighted average of the shifts for each spectral order. The dispersion of each of these orders in the obtained measurements is the major source of uncertainty in the Doppler shifts. Furthermore, Doppler shift profiles are affected by two other effects that interfere with zonal wind measurements: the geometric projection factor (F), which results

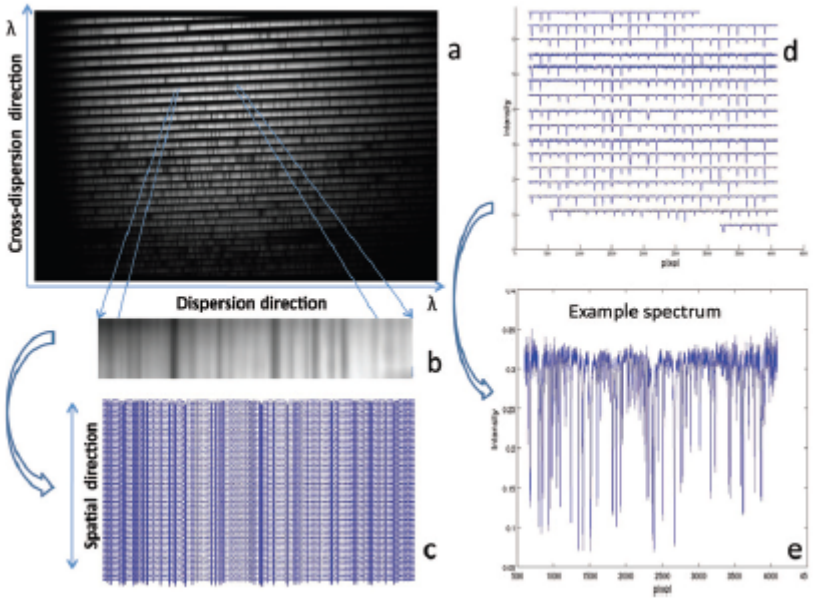

Figure 3.7: A UVES echellogramme example showing each step to obtain the desire spectra. First, in (a), we have the raw unprocessed echellogramme with the spectral orders. Next, in (b), we took part of one of these spectral orders and zoomed it to look at the absorption lines visible (dark vertical bands). In (c) we can see that each order contains a stack of 61 spectra, with each spectra corresponding to one pixel in the active window of the slit. Then, in (d), each spectrum is divided into 16 orders for the MIT detector and 23 orders for the EEV. Finally, in (e), the ends of each component are joined to get the final example spectrum from one order and one location in Venus's disc. From Pedro Machado et al. (2012)

from the observational spherical geometry; and the Young effect (Y), which results from the Sun's rapid rotation and its finite dimension as seen from Venus. Moreover, the relative orbital motion between Earth and Venus ($\approx -14 km/s$) must also be taken into account; the retrograde rotation of Venus could also be an important factor; however, since it is quite slow ($1.81 m/s$ at the equator) compared to the measured wind speeds, it can be ignored, as can the motion of particles in the clouds relative to the ground. Thus, the absolute Doppler shift measured along the line of sight at any point along the slit is (Pedro Machado, 2014):

$$\Delta V = F \cdot V + Y + OS \tag{3.9}$$

The orbital shift (OS) caused by the orbital motion between Earth and Venus is the same for each point of the slit. So, if we are calculating the relative Doppler shift between two spectra from the same observation, one from any probed point and the other from the reference point at the center of the slit, the orbital shift is canceled (Pedro Machado, 2014).

For simplicity, we assume that Venus is in its greatest eastern elongation, near quadrature (90^o phase angle), and the atmospheric motion is exclusively zonal in the retrograde sense. Two extreme cases are considered (see Figure 3.8a). One in the sub-solar point, where no Doppler shift is measured in the absorption, the direction of the incident light is perpendicular to that of the motion of the particles, but a blueshift is measured in the re-emission towards Earth, because the radiation is emitted tangent to the surface in the direction of the observer as the particles are approaching in its line of sight. Other at the subterrestrial point, where a redshift is measured in the absorption, because the radiation falls tangent to the surface in the same direction as the motion of the particles that move away from the Sun's line of sight, but no Doppler shift is measured in the emission, the direction of the emitted light is normal to the surface and perpendicular to that of the motion of the particles. The geometric projection factor (F) that affects the Doppler shift can be calculated and depends on the specific observing geometry and longitude

3. METHOD

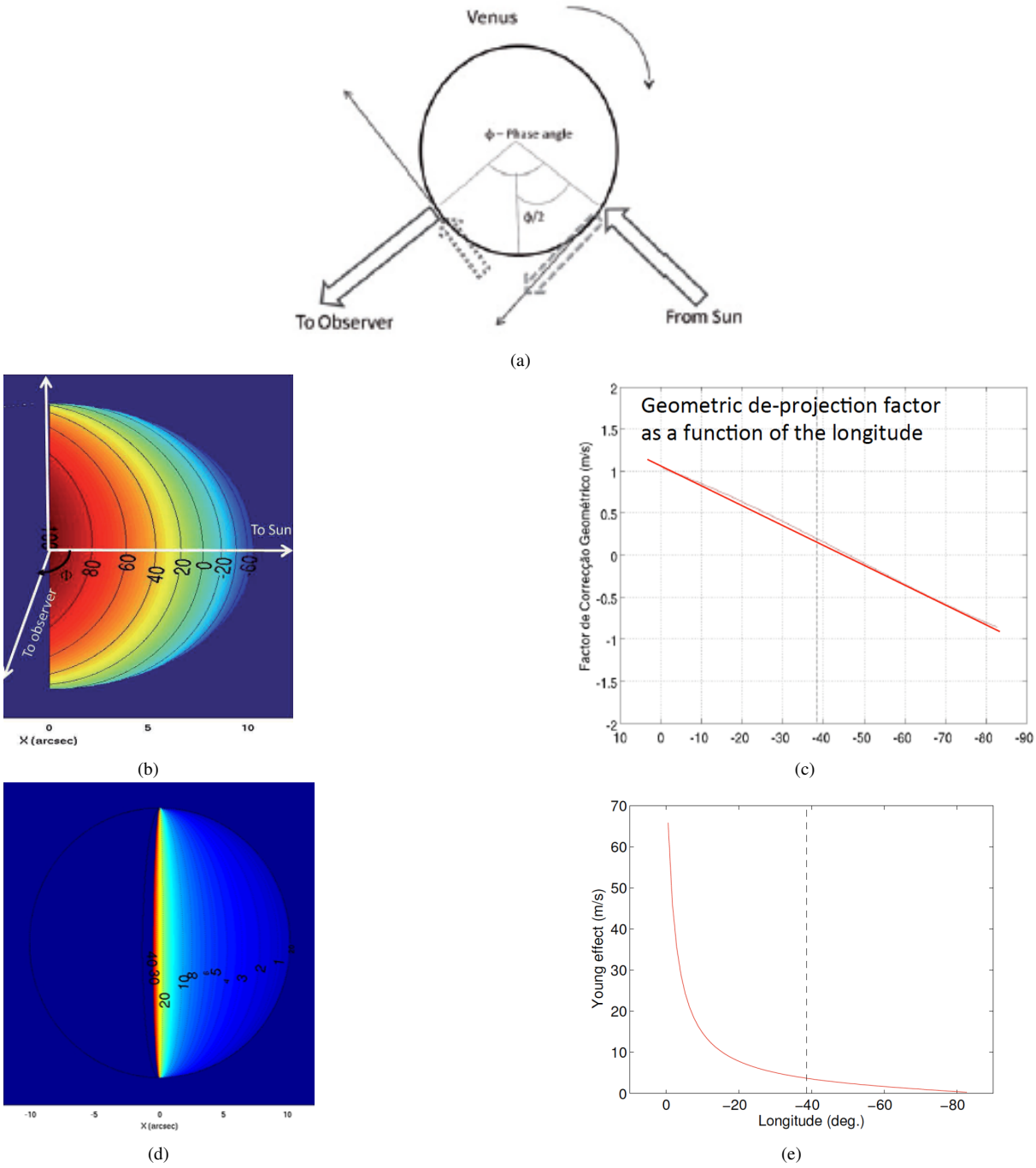

Figure 3.8: Representation of the Doppler effect (a), the dotted arrow in the sub-terrestrial point represents the redshift in the absorption of solar radiation and the dashed arrow at the sub-solar point represents the blueshift in the emission of solar radiation towards the observer, thin arrows represent the direction of zonal wind motion. Iso-lines for the geometric projection factor (b) and Young effect (d). Respective exemple behaviors for the de-projection factor (c) and Young effect (e) as function of longitude. From Pedro Machado et al. (2012) and Pedro Machado (2014).

(Pedro Machado, 2014) (Gabsi et al., 2008).

$$F = 2\cos(\Phi/2)\sin(\varphi - \Phi/2)\cos(\beta) \tag{3.10}$$

Φ is the phase angle at which the observation is made, β is the latitude of the subterrestrial point and φ is the longitude of the measured point that increases in the direction of rotation. The projection factor is null at the $\Phi/2$ longitude, near -45^o (see Figure 3.8b and Figure 3.8c), because the redshift produced

in the absorption cancels the blueshift of the emission (see Figure 3.8a). The Young effect is due to the finite angular size of the Sun as seen from Venus and its rapid rotation, which causes points near the terminator to be illuminated disproportionately between the approaching and receding limbs of the Sun (Young, 1975). Radiation from the former (western side) carries with it an intrinsic blueshift, and that from the latter (eastern side) carries an intrinsic redshift. The solar zenith angle varies with longitude, so points at different longitudes are illuminated differently by the blue-shifted part of the Sun and the red-shifted part, meaning that the average solar radiation may be shifted (Pedro Machado, 2014).

$$Y = \frac{V_{\odot} \cdot D_{\odot}}{\sin\theta} = 3.2\tan(SZA) \tag{3.11}$$

$V_{\odot}$ is the solar equatorial velocity ($2km/s$), $D_{\odot}$ is the solar angular diameter seen from Venus, θ is the angular distance between the observed point and the terminator, and SZA is the solar zenith angle (Young, 1975) (Gabsi et al., 2008). The Young effect is only significant near the terminator (see Figure 3.8d and Figure 3.8e), where the asymmetry in the solar radiation received is greater. It is probable that this correction of the Young effect fails near the limbs, in particular at high latitudes, since it is a purely geometric correction weighted by the illumination that is not proportional to the scattered intensity if there is a multiple scattering (Pedro Machado, 2014).

3.3.2 The database

All data used to feed the algorithm were obtained from the ESO archive, in the raw data search section. In the query form, we simply entered the Program ID and a time range capable of encompassing all three observation nights (August 20th, August 29th, and September 3rd). Regarding data categories, we requested all data types: science, acquisition, and special calibration (European Southern Observatory, 2025b).

After requesting all this data and before download, we ran association of the associated processed calibrations (the set of master processed calibrations needed to process the raw science files) and the associated raw calibrations (the set of raw calibrations needed to process the raw science files - ARC) (European Southern Observatory, 2025b).

The next step was to open each of these files, one by one, and choose only those that held the following configuration: cross-disperser *CD*#3; dichroic mode 1; central wavelength 580nm and the below-slit filter SHP700. The entire algorithm had been built and adapted to this configuration, so we kept the same characteristics.

For the science and slit image files, we had to remove some files whose targets were not Venus, but reference stars like RHO CEN and 108 VIR. From the ARC files, we obtained all the data for the bias, flat-field, and calibration lamp folders. We also needed order definition files; to obtain them, we had to perform a new search in the ESO archive, this time not using the Program ID, but searching only by date and instrument. Last but not least, the mask and wavelength calibration files were reused from previous works that used this same algorithm. This way, our database is completed, for each exposure we have:

- 1 science frame;
- 1 slit image viewer frame (there is one for each science);
- a set of 5 bias frames (each set for each night of observation);
- a set of 5 flat filed frames (each set for each night of observation);

- 1 lamp frame (one for each night of observation);
- 1 order definition frame (one for each night of observation);
- 1 mask zip file (the same for all exposures);
- 1 wavelength calibration file (the same for all exposures);

From the first night we have 9 exposures and from the other two 18 exposures each, giving a total of 45 scince frames. The calibration data are the same for a given night. All these data will be stored in one Database function that contains all the required data in order to process the observations, including the data paths, some instrument settings, target diameter, pixel scale, etc... and it will be called one time at the begining of each data reduction. The majority of these data reduction is handled by the WIND software package (Thomas Civeit, 2004).

3.3.3 WIND software package

WIND is a software package developed for the MATLAB computing environment. It is dedicated to spectroscopic measurements of planetary winds, exactly what we are doing here, and consists of main and core procedures. More information can be found at T. Civeit et al. (2005). The package comes with different functions, each responsible for a different data processing task. All of them are grouped in a hierarchical order and are called by each other in a logical sequence in routines and subroutines. Here is the most probable order of use (Thomas Civeit, 2004):

- **wind target.m** - This is the first function and the only one that we call from the command window. It encompasses all the other functions, it sets the directory paths, loads the database, and runs the data reduction for the selected observations;
- **wind check.m** - This function is called by the previous one. It makes sure that all the necessary files are there and are readable and it is the responsable for the median master frames of the bias and flat field frames. When images are large, it can take several minutes to median filter pixel-by-pixel, so, the median frames are saved to prevent wasting time on subsequent data processing.
- **wind main target.m** - As the name says, this is the most important function, it is also called by the first one and it will call all the following ones. It is the center of the entire operation, it defines which steps must be performed (import files, map order locations, estimate scattered light, extract spectra, compute Doppler shifts and plot results). The set of steps is sequentially performed. All subsequent functions are called from this one, each one performing a task required for the data reduction.
- **wind import.m** - It imports, formats and saves the science, flat field, lamp, CCD bad pixel mask and order definition frames data in the working directory as MATLAB ".mat" files. After this, they start being loaded from the back-up and not from the original file, making them easier to open and use.
- **wind map.m** - It determines the echelle order locations, performing an image segmentation in order to detect the peaks of intensity, then it fits the order traces with a 2nd degree polynomial.
- **wind scat.m** - It estimates the scattered light and sky emission on the CCD by performing inter-order measurements and interpolation.

- **wind x2d.m** - It extracts the 2D spectrum from each order.
- **wind lcurv.m** - It estimates the slit image curvature by using an optimum weight algorithm.
- **wind wave.m** - It fits the line positions given by the calibration table with a 2nd degree polynomial in order to compute the dispersion solution. It calibrates with the Th-Ar lamp to assign pixels to wavelengths (dispersion relation).
- **wind doppler.m** - It computes the Doppler shifts. It requires the dispersion relation (polynomial coefficients previously computed).
- **wind multidop.m** - It computes spatial velocity changes using the same optimum weighted algorithm than the previous function, but considering adjacent peers of spectra (reference + shifted) along the slit.
- **wind plot.m** - It plots the results, which consist in the estimates of scattered light, the slit image curvature, the Doppler shifts relative to the slit center, the differential Doppler shifts at different regions and the irradiance profile.

After running the WIND software package we get the Doppler shifts relative to the reference spectrum, corresponding to the centre of slit, this means we only have the relative winds and not absolute. The next step will be to convert the pixels of the slit into venusian longitude and latitude. This is a crutial and precise step since we have to find out the coordinates of all the pixels in the slit for each exposure. This is also the part where the geometric projection factor and Young effect are calculated and corrected. Only knowing the latitude of the slit, and the longitude of each pixel, we can convert those relative wind into absolute ones.

3.3.4 The proposal and the chosen exposure

From this stage forward we will only focus in one exposure from the first night (August 20^{th}). This exposure is the 9^{th} and last exposure from this date, so we will call it $K9$ (see Figure 3.9). All the other exposures will later be addressed in future works and in a possible follow-up to this thesis. From here, we stopped using the algorithm and we started manipulating the results manually using an Excel spreadsheet. We obtained the relative Doppler shifts from the previous section and now it remained to calculate the deprojection factors and youth effects for each pixel, apply them to the Doppler shifts and finally obtain the absolute velocities for the zonal winds of Venus.

The proposal made for this observation tried to maximize as much as possible the period of observability due to maximum target elevation after sunset, with the target trailing the sun and setting after it (European Organisation for Astronomical Research in the Southern Hemisphere, 2017). The elongation is also near the maximum in order to optimise observations: the solar elongation angle (Sun-Observer-Target) is near 46^o. For the chosen exposure (K9), the target has an apparent magnitude of -4.47, an angular diameter of $25.33''$ and an illuminated fraction of 46.89%, which corresponds to a surface brightness of $SB = 1.464 \quad mag/arcsec^2$. The moon is about 75.2% illuminated by the Sun and the lunar elongation angle is near 74.5^o with the refracted upper-limb of the moon on or above apparent horizon, the sky brightness due to moonlight scattered by Earth's atmosphere at the target's position in the sky is $1.55 \quad mag/arcsec^2$. The event occurs in astronomical twilight, with Airmass = 2.11, extinction = 0.3, seeing = 0.5" and exposure time = 1 second. All these values were retrived from the exposure header and from NASA Jet Propulsion Laboratory (2024), using Venus as target body, Paranal Observatory (VLT) as observer location and the time specification range corresponding to $K9$

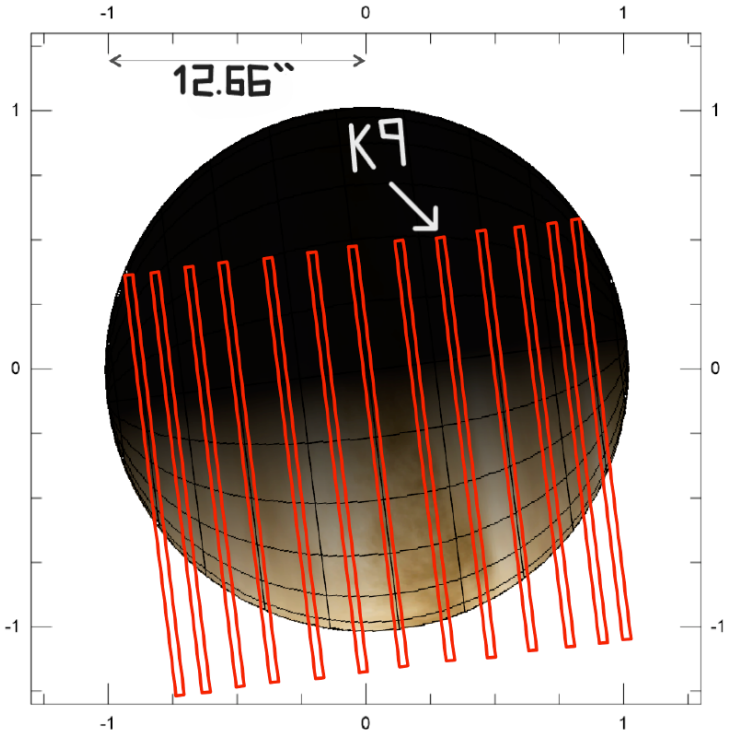

Figure 3.9: Observation proposal made for this set of observations with UVES that consisted of 13 different slit positions, perpendicular to Venus's rotation axis (PP), covering the latitude parallels from -60º to +60º, with a separation of 10º (corresponding to separations of 2"). From European Organisation for Astronomical Research in the Southern Hemisphere (2017). We consider the *K*9 to be in the latitude slit position of 20^o North. In this image we can see the total slit window of 20 arcseconds, but we only get results from the active window which as only 12 arcseconds.

Table 3.1: North Pole position angle, apparent radius of Venus, latitude of sub-solar point and phase angle at the time of the K9 exposure. From NASA Jet Propulsion Laboratory (2024)

Position Angle (º)	Apparent Radius (")	Sub-Solar Latitude (º)	Phase Angle (º)
22.56	12.66	2.00	93.57

3.3.5 From relative Doppler shifts to absolute velocity winds

At this stage of the work, and until we reach the final results, we will make a very important approximation. We will assume that the pixel that falls in the center of the slit, corresponds to the point on Venus whose longitude is equal to half the phase angle. The Phase Angle (PA) corresponds to the angle between the vector that leaves Venus towards the center of the Sun and the vector that leaves Venus towards the observation point on Earth (VLT). In this point, it is never possible to measure velocity, which corresponds to the point without measured relative Doppler shift, because it is precisely the center of the slit:

$$\Phi_{PA} = -93.57^o \quad \Longrightarrow \quad Lon_{c.px} = \frac{\Phi_{PA}}{2} = -46.785^o \tag{3.12}$$

Each pixel in the slit, and its corresponding points on Venus's disc, are equally spaced, so by taking the coordinates of the central point ($Lon_{c.px} = -46.785^o \quad Lat_{c.px} = +20^o$), we can reach all the others. It's worth remembering that the slit is positioned perpendicular to Venus's axis of rotation (PP), so its latitude is constant and shared by all points. Since the slit has a 0.3" width and covers a latitude band of 2.4^o at disc center, the latitude value has an uncertainty of 1.2^o.

Table 3.2: Table showing the relative Doppler shift obtained from the algorithm and respective error, we also displayed the slit region by pixel and the corresponding place in the planetary disc. The shift error increase along the slit is due to the curvature of the planet, pixels closer to the limb detect radiation that passes through a more extensive layer of the atmosphere and therefore undergoes greater scattering

Slit region (px)	Rel. Doppler shift (m/s)	Rel. Dop. shift error (m/s)	Planetary disc region
-10	154.469638	2.706163	nightside
-9	151.548912	2.705297	nightside
-8	141.973315	2.708501	terminator
-7	130.407699	2.712852	dayside
-6	116.678656	2.716884	dayside
-5	101.634126	2.724439	dayside
-4	84.578272	2.725584	dayside
-3	64.742611	2.728067	dayside
-2	44.369898	2.726104	dayside
-1	22.070965	2.725421	dayside
0	0	2.728077	central slit pixel
1	-20.030346	2.744014	dayside
2	-42.150231	2.754658	dayside
3	-61.260802	2.751896	dayside
4	-81.570635	2.749683	dayside
5	-100.440266	2.754129	dayside
6	-116.740417	2.757132	dayside
7	-131.488609	2.753869	dayside
8	-143.514803	2.748576	limb
9	-152.571126	2.743793	outside
10	-159.71945	2.743263	outside

To calculate the deprojection factor and Young effect (only in the dayside), assuming the approximation that the central point corresponds to half the PA, we use the models presented in Figure 3.7 (c) and (e), respectively. For the Young effect, after assigning each point its longitude, we also assign the corresponding Young effect to that longitude. For the deprojection factor, we assume an almost linear two-branch relation where the central point corresponds to the null factor point and from there, the function increases linearly for longitudes closer to the terminator until reaching unity; the opposite occurs, almost but not symmetrically, for longitudes closer to the limb. It is worth remembering that in this work, we are assuming a two-dimensional geometry for the planetary disc of Venus. This geometry is more effective and accurate at longitudes close to zero, because the closer we get to the limb, the faster the longitudes decrease (or increase, depending on the hemisphere), the same happens with the latitudes. Now we have everything we need to get the velocities for each point:

$$\begin{aligned} \Delta V_i &= F_i \cdot V_i + Y_i \\ \Delta V_o &= F_o \cdot V_o + Y_o \end{aligned} \tag{3.13}$$

The index "i" represents each pixel along the slit for each case and the index "o" refers to the central point pixel at the slit. The quantity representing the relative Doppler shift is:

$$\Delta V_i - \Delta V_o = F_i \cdot V_i + Yi - (F_o \cdot V_o + Yo) \tag{3.14}$$

Since the slit is aligned perpendicularly to the rotation axis (PP), it lies entirely in one single lati-

Table 3.3: Table showing the Longitude, Young effect and De-projection factor given for each pixel in the dayside

Slit region (px)	Longitude (º)	Young effect	De-projection factor
-7	-9.475	15.29	1.000
-6	-14.805	10.29	0.950
-5	-20.135	7.94	0.792
-4	-25.465	5.88	0.634
-3	-30.795	4.71	0.476
-2	-36.125	3.82	0.318
-1	-41.455	3.24	0.160
0	-46.785	2.35	0
1	-52.115	2.06	-0.272
2	-57.445	1.76	-0.408
3	-62.775	1.47	-0.544
4	-68.105	1.18	-0.680
5	-73.435	0.88	-0.816
6	-78.765	0.59	-0.952
7	-84.095	0.29	-1.000

tudinal ring on Venus, and under the assumption that the zonal wind depends only on latitude, we can presume that it will be constant or it must be nearly constant. So, $V_i = V_o = V$, which gives us (Pedro Machado, 2014):

$$V = \frac{\Delta V_i - \Delta V_o - Yi + Yo}{F_i - F_o} \tag{3.15}$$

In the next section, we'll display the results, then we will have a general discussion and get to final conclusions.

Table 3.4: Summary of the geometry and circunstances of the observations. The integration time for all exposures was 1 second. Lat and Long are the coordinates of the slit's central point on the disc and their values are affected by the VLT/UVES nominal pointing and offset uncertainty, with a total uncertainty of 0.14".

Slit	Offset	Date (dd-mm-yy)	Time UT	Lat	Long	Airmass	Seeing (")
PP	9	20-08-18	23:41:32	20 N	46.785 E	2.113	0.55

3.4 Results

In this section I present the velocity wind measurements retrieved for the chosen exposure K9 with the slit perpendicular to the rotation axis. This type of observation allows to measure the absolute magnitude of the wind velocity as the pixels along the slit all fall on the same latitude circle. We assume that the zonal wind depends only on latitude, so, we can obtain the zonal wind directly from the longitudinal profile of the relative velocity. The measured spectrum and the reference spectrum (from slit's center) are not at the same SZA (solar zenith angle), so, the correction for the de-projection factor and Young effect, both dependent on longitude, had to be made. The de-projection factor falls to zero and changes sign close to the slit center, and since the correction is made by dividing the relative shift by it, this region will have higher uncertainty and the error bars will be wider. (Pedro Machado, 2014).

As we can see in Figure 3.10, the velocities are nearly constant, ranging from 81 to 131 m/s. However, we should discard the upper extreme because it is too close to the limb, where radiation scattering is greater due to more atmosphere crossed, we also should discard the lower extreme because it is too close to the slit centre where the results tend to diverge and the uncertainty is higher. By doing this the velocities will only range between 20m/s. The uncertainty can also be caused by local variations that cannot be observed or monitored because the results refer only to one latitudinal ring; more would be needed to detect them and study their pattern. In general, the zonal wind is approximately uniform for each latitude circle, in accordance to our initial assumption at first order. (Pedro Machado, 2014)

According to studies conducted in (Pedro Machado et al., 2012), (Pedro Machado, 2014), (P. Machado, Widemann, J. Peralta, et al., 2014), (P. Machado, Widemann, Peralta, et al., 2017) and (Gonçalves et al., 2020), latitudes closer to the equator should have higher zonal wind speeds when compared to high latitudes but lower when compared to mid-latitudes. Our measured latitude, K9 (20º North), lies between the equator and mid-latitudes, therefore, if the same process were repeated for the other positions of the slit (see Figure 3.9) and the results were obtained, the velocity values for this exposure would be neither the highest nor the lowest. From here the wind speeds should descend towards the equator but should increase towards mid-latitudes (near 40º), and then decrease again in even higher latitudes. Because we are only focusing on one latitude, it is not possible to find comparative patterns to recognize some small or medium-scale local oscillations, but they exist and should not be neglected. The magnitude of these (second order) oscillations cannot be quantified directly, since our retrievals are based on the working hypothesis that the zonal wind does not depend on longitude (Pedro Machado, 2014).

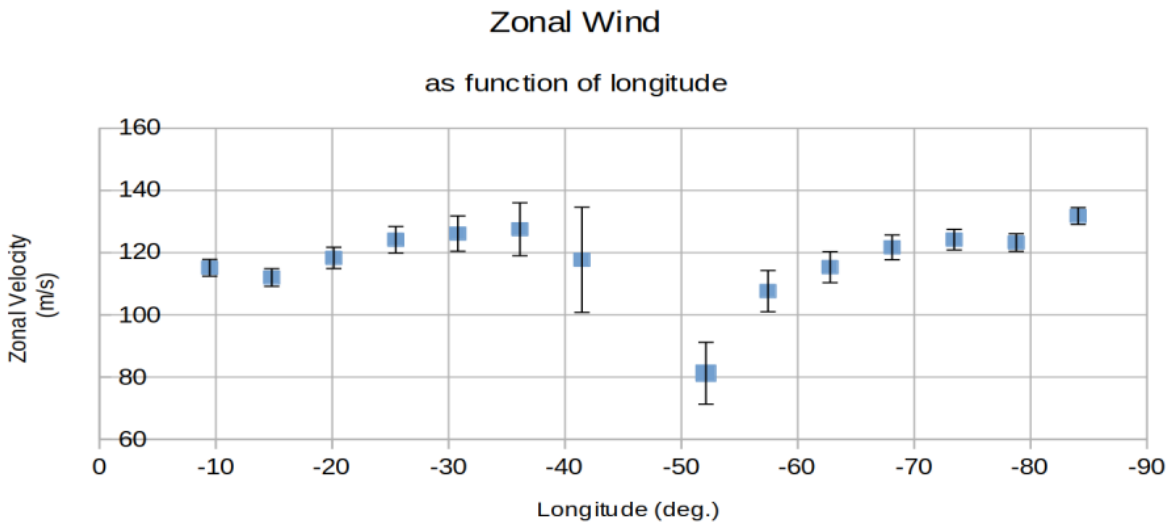

Figure 3.10: Zonal wind versus longitude for the 9^{th} observation (K9) made at August 20^{th} 2018 with the spectroscopic slit parallel to the equator. We are only considering the MIT detector. The slit latitude is 20 N and the central slit longitude is 46.785 E.

This VLT/UVES long-slit result is complementary to the results obtained from the observations carried out by previous studies using the Doppler Velocimetry technique and the same set of instruments to target Venus (Pedro Machado et al. (2012); Pedro Machado (2014)). The UVES long-slit measurements allowed to yield an instantaneous wind latitudinal profile.

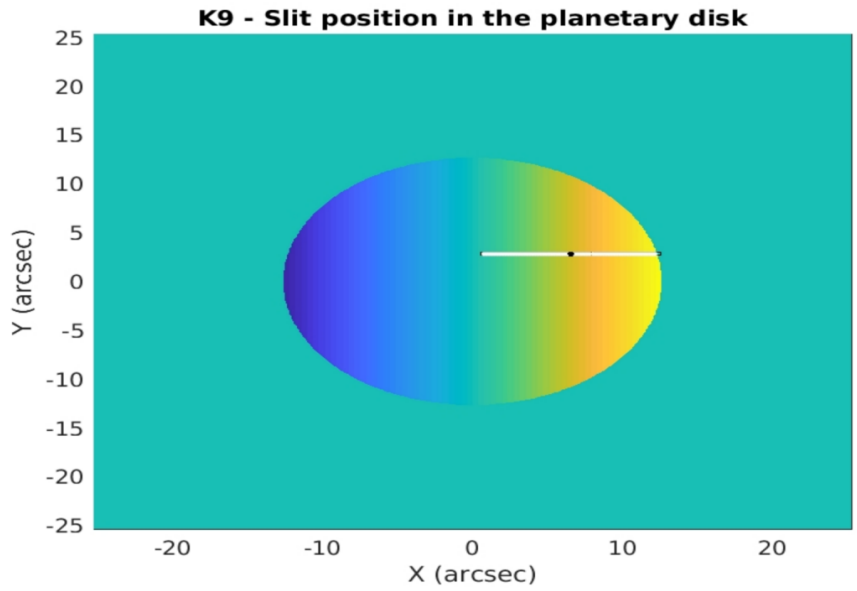

Figure 3.11: Slit's position scheme on the planetary disc, with an apparent radius of 12.66", for the K9 case. It is only shown the active window of the slit on the dayside with 12 arcseconds.

Table 3.5: Latitude covered and mean zonal wind velocity measured for the K9 exposure with the PP geometry. Std. Dev. is the standard deviation of the weighted mean. The latitude is given for the slit center with an uncertainty of 1.2º; the 0.3"-slit covers a latitude band of 2.4º at disc center.

Latitude	Zonal Velocity (m/s)	Std. Dev. (m/s)
20º North	117.56	11.29

Chapter 4

Discussion, conclusions and future work

The velocity retrievals in Figure 3.10 are in general in a good agreement and in the same order of magnitude with previous measurements based on cloud tracking (Del Genio et al. (1990); Limaye (2007); J. Peralta et al. (2007); A. Sánchez-Lavega et al. (2008); Moissl et al. (2009)) cross-validating both alternatives and confirming that the cloud tracking technique and the Doppler velocimetry method can both retrieve the velocities of atmosphere winds to first order.

The discrepancies between the two techniques can be due to the latitudinal wind profiles of cloud tracking being made by using a wide range of longitudes for the average of too many measurements of velocities of individual clouds, while our Doppler technique directly measures the instantaneous velocity of cloud particles within a particular range of local solar time. This local property of the Doppler measurements most likely accounts for the discrepancy, due to the presence of thermal tides. This thermal tide contribution can be averaged out if the data is available over the complete longitude circle, but, again, our measurements are local and sensitive to solar-locked extrema (Pedro Machado, 2014).

Instead of being discrepant, the different wind measurements provided over the years and using different techniques, gives the cientific community important insight about the variability inherent to the atmospheric circulation of Venus. Our direct measurements of instantaneous zonal winds provide extra evidence for the occasional and short-term presence of jets and for variability in general, while the cloud tracking gives us a more detailed and extensive understanding of the evolution of these jets as it is done over a longer period of time. There is still doubt about the role of the mean meridional circulation on the formation of these jets, and their relation to long-term structures like the polar vortex and its surrounding cold collar (Pedro Machado, 2014).

The case where we have an observing geometry with the slit parallel to the rotation axis (PL) gives us relative wind measurements (relative to the reference point - slit centre), whereas the PP case, with the slit perpendicular to the rotation axis, provides absolute wind measurements. Therefore, if we had the two different configurations, we could have used the mean values of the winds measured for each PP offset to calibrate the PL curve, where the wind at the reference point is null. This would allow to obtain both longitudinal and latitudinal profiles, unfortunately, the observation proposal did not include the PL configuration. So, the best we can do, in future work, is to repeat the same procedure to all 45 exposures that we all at disposal and then, using the average wind speed values at each latitude cicle, we plot a correlation curve that relates the wind speed to the range of latitudes covered. However, that will only be possible if we continue working on this topic and with this data. It will also be possible to study and detect large-scale planetary waves or small to medium-scale local oscillations, and even to study other types of atmosphere circulations like the Hadley circulation. The observation of small scale perturbations could indicate that small scale wave motions are the most likely process by which the instability unfolds.

4. DISCUSSION, CONCLUSIONS AND FUTURE WORK

Future studies about wave motions and their latitudinal flows of angular momentum should focus in the mid-latitudes.

The Doppler velocimetry tecnique based on long slit spectroscopy with the VLT/UVES instrument has already enabled the retrieval of ground-based direct measurements of instantaneous latitudinal profile of zonal winds in the atmosphere of Venus before (Pedro Machado et al. (2012); Pedro Machado (2014)), and now we successfully did it again using a new set of data from 2018. We proved again that this technique allows to retrieve zonal winds across a range of longitudes and local times. The detection of local small scale variations relative to the background mean zonal wind stays dependent on the subsequent and plausible future follow-up of this thesis when determining the remaining zonal winds at the other available latitudes; only then we will have a clearer view of the evolution of the zonal wind in both longitude and latitude, and of the presence of local oscillations.

The results are consistent with previous wind field retrievals based on both Doppler velocimetry and cloud tracking observing the same region of the planet (Pedro Machado et al., 2012) (P. Machado, Widemann, J. Peralta, et al., 2014) (P. Machado, Widemann, Peralta, et al., 2017) (Gonçalves et al., 2020). The near instantaneous property of the Doppler velocimetry technique is important to better constrain Venus's atmospheric dynamics. So, spatial and temporal atmospheric surveys with the same or better accuracy when compared to space-based cloud tracking, can be made from the ground. The two methods of observation are complementary in both spatial coverage and temporal resolution and both should be equally considered as solutions to better understand the different aspects of cloud top dynamics.

Currently, the super-rotation of Venus's atmosphere is not yet fully understood. We have a vague idea of how it currently works, but we don't know how it reached this super-accelerated state, especially on a slowly rotating planet, and how this state is supported and maintained. The information is still not enough to constrain current models of zonal super-rotation.

With news that the construction of the ELT (Extremely Large Telescope) is progressing successfully and on schedule (European Southern Observatory, 2025a), we hope that in the near future we will be able to repeat these same observations, both for Venus and for Titan, Saturn or Jupiter, using this new and giant telescope with a diameter of 39m, and who knows, it may even be possible to reapply this method to the atmospheres of exoplanets with the help of ARIEL. We also have the new comming up space mission EnVision planned to launch at 2031 (European Space Agency, 2025), so, we are looking forward for the next decade and the new possibilities and observation tools that it will have for us. More extensive temporal surveys and better spatial resolution are two key parameters in order to finally reveal the secrets of our evil twin sister planet.

To summarize, the Doppler velocimetry method in the visible range is the best option in the ground-based regime to constrain the atmospheric global circulation, considering Venus's RZS at times scales on the order of one hour to several days, since instantaneous winds are retrieved. It helps constructing a 3D model of the wind velocity field that uses results from different altitudes and techniques, both ground and space based. When the datasets overlap, the Doppler velocimetry technique and the cloud tracking technique cross validate themselves, so, it is useful to join both techniques in coordinated observing studies. It is important to keep measuring winds at different altitudes and at all latitudes, from both ground and space based tecniques, in order to better understand and constrain the dynamics of Venus's atmosphere.

Bibliografia

Abel, Paul G. (2017). “Astronomical Seeing Part 1.” In: *British Astronomical Association*.

Blamont, J. (2008). “Planetary balloons”. In: *Experimental Astronomy* 22.1, pp. 1–39. DOI: 10.1007/s10686-008-9095-8.

Bougher, S. W., M. J. Alexander, and H. G. Mayr (1997). “Upper Atmosphere Dynamics: Global Circulation and Gravity Waves”. In: *Venus II: Geology, Geophysics, Atmosphere, and Solar Wind Environment*. Ed. by S. W. Bougher, D. M. Hunten, and R. J. Phillips. Tucson: University of Arizona Press, pp. 259–291.

Bullock, M. A. and D. H. Grinspoon (2001). “The recent evolution of climate on Venus”. In: *Icarus* 150, pp. 19–37. DOI: 10.1006/icar.2000.6570.

Civeit, T. et al. (2005). “On measuring planetary winds using highresolution spectroscopy in visible wavelengths”. In: *Astronomy and Astrophysics* 431.3, pp. 1157–1166. DOI: 10.1051/0004-6361:20041640.

Civeit, Thomas (Sept. 2004). *WIND User’s Manual*. Version 1.0. Available upon request from the author.

Clancy, R.T., B.J. Sandor, and G. Moriarty-Schieven (2012). “Thermal structure and CO distribution for the Venus mesosphere/lower thermosphere: 2001–2009 inferior conjunction sub-millimeter CO absorption line observations”. In: *Icarus* 217.2, pp. 779–793. DOI: 10.1016/j.icarus.2011.05.032.

Connes, Pierre (1985). “Absolute astronomical accelerometry”. In: *Astrophysics and Space Science* 110.2, pp. 211–255. DOI: 10.1007/BF00653671.

Cornish, Paul (2025). “Where can I find planet Venus?” In: *We the curious*.

Cottini, V. et al. (2012). “Water vapour near the cloud tops of Venus from Venus Express/VIRTIS dayside data”. In: *Icarus* 217.2, pp. 561–569. DOI: 10.1016/j.icarus.2011.06.018.

Crisp, D. et al. (1990). “VEGA balloon meteorological measurements”. In: *Advances in Space Research* 10.5, pp. 109–124. DOI: 10.1016/0273-1177(90)90172-V.

D’Odorico, Sandro et al. (2000). “Performance of UVES, the echelle spectrograph for the ESO VLT and highlights of the first observations of stars and quasars”. In: *Discoveries and Research Prospects from 8- to 10-Meter-Class Telescopes*. Vol. 4005. Proceedings of SPIE, pp. 121–130. DOI: 10.1117/12.390133.

Dekker, Hans et al. (2000). “Design, construction, and performance of UVES, the echelle spectrograph for the UT2 Kueyen Telescope at the ESO Paranal Observatory”. In: *Optical and IR Telescope Instrumentation and Detectors*. Ed. by Masanori Iye and Alan F. Moorwood. Vol. 4008. Proceedings of SPIE, pp. 534–545.

Del Genio, A. D. and W. B. Rossow (1990). “Planetary-scale waves and the cyclic nature of cloud top dynamics on Venus”. In: *Journal of the Atmospheric Sciences* 47, pp. 293–318. DOI: 10.1175/1520-0469(1990)047<0293:PSWATC>2.0.CO;2. URL: https://www.sciencedirect.com/science/article/abs/pii/S0019103516304328.

Dollfus, A. (1975). “Venus: evolution of the upper atmospheric clouds”. In: *Journal of the Atmospheric Sciences* 32, pp. 1060–1070. DOI: 10.1175/1520-0469(1975)032<1060:VEOTUA>2.0.CO;2.

Dorn, Reinhold J. et al. (2000). “Optical detector systems of UVES: the echelle spectrograph for the UT2 Kueyen Telescope at the ESO Paranal Observatory”. In: *Optical and IR Telescope Instrumentation and Detectors*. Ed. by Masanori Iye and Alan F. Moorwood. Vol. 4008. Proceedings of SPIE, pp. 344–355. DOI: 10.1117/12.395492.

ESO Education Office (2004). *Venus - the second planet of the solar system*. European Southern Observatory. URL: https://www.eso.org/public/outreach/eduoff/vt-2004/Background/Infol1/BIS-D1.html.

Espaço do Conhecimento UFMG (2022). *Planeta Vênus e as semelhanças com a Terra*. Site institucional, Espaço do Conhecimento UFMG. Acessado em 11 de junho de 2025. URL: https://www.ufmg.br/espacodoconhecimento/planeta-venus-e-as-semelhancas-com-a-terra/.

Esposito, L. W. et al. (1983). “The Clouds and Hazes of Venus”. In: *Venus*. Ed. by D. M. Hunten et al. Tucson, AZ: University of Arizona Press, pp. 484–564. ISBN: 9780816507887.

European Organisation for Astronomical Research in the Southern Hemisphere (2017). *Unknown ultraviolet absorber in Venus' atmosphere - Application for Observing Time, Period 99A*. ESO Observing Programmes Office, Garching bei München. Proposal submitted by P. Machado, Y. Lee, J. Peralta, R. Gonçalves, and T. Widemann.

European Southern Observatory (2007). *Very Large Telescope Paranal Science Operations UV-Visual Echelle Spectrograph User manual*. VLT-MAN-ESO-13200-1825. European Southern Observatory. Garching bei München, Germany / Paranal Observatory, Chile.

— (2025a). *ELT Timeline*. https://elt.eso.org/about/timeline/. Accessed on 17 November 2025.

— (2025b). *ESO Science Archive Facility*. URL: https://archive.eso.org/.

European Space Agency (Dec. 2014). *Venus Express goes gently into the night*. News release on ESA website. Mission officially declared ended 16 December 2014. URL: https://www.esa.int/Science_Exploration/Space_Science/Venus_Express/Venus_Express_goes_gently_into_the_night.

— (Nov. 2020). *Ariel Definition Study Report (Red Book)*. ESA/SCI(2020)1. Published 12 November 2020. Paris, France: European Space Agency. URL: https://sci.esa.int/documents/34022/36216/Ariel_Definition_Study_Report_2020.pdf.

— (Jan. 2025). *EnVision mission factsheet*. ESA website. URL: https://www.esa.int/Science_Exploration/Space_Science/Envision/Envision_factsheet.

Gabsi, Younes et al. (2008). “Measuring Venus' winds using the Absolute Astronomical Accelerometer: Solid super-rotation model of Venus' clouds”. In: *Planetary and Space Science* 56, pp. 1454–1466. DOI: 10.1016/j.pss.2008.04.011.

Gonçalves, Ruben et al. (2020). “Venus' cloud top wind study: Coordinated Akatsuki/UVI with cloud tracking and TNG/HARPS-N with Doppler velocimetry observations”. In: *Icarus* 335, p. 113418. DOI: 10.1016/j.icarus.2019.113418.

Goody, R. M. and J. C. G. Walker (1975). *Atmosferas Planetárias*. Brasil: Edgard Blücher.

Grinspoon, D. H. (1997). *Venus Revealed: A New Look Below the Clouds of Our Mysterious Twin Planet*. Cambridge, Massachusetts: Helix Books (Perseus Publishing).

Hueso, R., J. Peralta, and A. Sánchez-Lavega (2012). “Assessing the long-term variability of Venus winds at cloud level from VIRTIS–Venus Express”. In: *Icarus* 217.2, pp. 585–598. DOI: 10.1016/j.icarus.2011.04.020.

Kak, Subhash C. (1996). "Vena, Veda, Venus". In: *Brahmavidyā: The Adyar Library Bulletin* 60, pp. 229–239.

Kargel, J. S. et al. (1994). "Carbonate-Sulfate Volcanism on Venus?" In: *Icarus* 112.1, pp. 219–252. DOI: 10.1006/icar.1994.1179.

Knollenberg, R. G. and D. M. Hunten (1980). "The Microphysics of the Clouds of Venus: Results of the Pioneer Venus Particle Size Spectrometer Experiment". In: *Journal of Geophysical Research* 85.A13, pp. 8039–8058. DOI: 10.1029/JA085iA13p08039.

Lellouch, E. et al. (1997). "Monitoring of mesospheric structure and dynamics". In: *Venus II: Geology, Geophysics, Atmosphere, and Solar Wind Environment*. Ed. by S. W. Bougher, D. M. Hunten, and R. J. Phillips. Tucson, AZ: University of Arizona Press, pp. 295–324. ISBN: 978-0-8165-1830-2. DOI: 10.1016/j.pss.2007.01.004.

Limaye, S. S. (1985). "Venus atmospheric circulation: Observations and implications of the thermal structure". In: *Advances in Space Research* 5.9, pp. 51–62. DOI: 10.1016/0273-1177(85)90270-4.

— (2007). "Venus atmospheric circulation: Known and unknown". In: *Journal of Geophysical Research: Planets* 112, E04S09. DOI: 10.1029/2006JE002814. URL: https://doi.org/10.1029/2006JE002814.

Luz, D. et al. (2006). "Characterization of zonal winds in the stratosphere of Titan with UVES: 2. Observations coordinated with the Huygens Probe entry". In: *Journal of Geophysical Research: Planets* 111, E08S90. DOI: 10.1029/2005JE002617.

Machado, P., T. Widemann, J Peralta, et al. (2017). "Venus cloud-tracked and doppler velocimetry winds from CFHT/ESPaDOnS and Venus Express/VIRTIS in April 2014". In: *Icarus* 285, pp. 8–26. DOI: 10.1016/j.icarus.2016.12.017. URL: https://www.sciencedirect.com/science/article/abs/pii/S0019103516304328.

Machado, P., T. Widemann, J. Peralta, et al. (2014). "Wind circulation regimes at Venus' cloud tops: Ground-based Doppler velocimetry using CFHT/ESPaDOnS and comparison with simultaneous cloud tracking measurements using VEx/VIRTIS in February 2011". In: *Icarus* 243, pp. 249–263. DOI: 10.1016/j.icarus.2014.08.030.

Machado, Pedro (2014). *Dynamics of Venus' Atmosphere, Characterization of its Global Circulation with Doppler Velocimetry*. Scholars' Press.

— (2024). *Planetary Systems*. Assisted classes in the course of Astrophysics at the Faculty of Sciences of the Univesity of Lisbon.

Machado, Pedro et al. (2012). "Mapping zonal winds at Venus's cloud tops from ground-based Doppler velocimetry". In: *Icarus* 221, pp. 248–261. DOI: 10.1016/j.icarus.2012.07.012.

Marcq, E., J.-L. Bertaux, et al. (2013). "Variations of sulphur dioxide at the cloud top of Venus's dynamic atmosphere". In: *Nature Geoscience* 6.1, pp. 25–28. DOI: 10.1038/NGEO1650.

Marcq, E., T. Encrenaz, et al. (2006). "Remote sensing of Venus' lower atmosphere from ground-based IR spectroscopy: Latitudinal and vertical distribution of minor species". In: *Planetary and Space Science* 54, pp. 1360–1370. DOI: 10.1016/j.pss.2006.04.024.

Markiewicz, W. J., D. V. Titov, N. I. Ignatiev, et al. (2007). "Venus Monitoring Camera for Venus Express". In: *Planetary and Space Science* 55.12, pp. 1701–1711. DOI: 10.1016/j.pss.2007.01.004.

Markiewicz, W. J., D. V. Titov, S. S. Limaye, et al. (2007). "Morphology and dynamics of the upper cloud layer of Venus". In: *Nature* 450.7170, pp. 633–636. DOI: 10.1038/nature06320.

Marov, Mikhail Ya. and David H. Grinspoon (1998). *The Planet Venus*. Yale Planetary Exploration Series. New Haven and London: Yale University Press, p. 442. ISBN: 9780300049756.

Moissl, R. et al. (2009). "Venus cloud top winds from tracking UV features in Venus Monitoring Camera images". In: *Journal of Geophysical Research: Planets* 114, E00B31. DOI: 10.1029/2008JE003117. URL: https://doi.org/10.1029/2008JE003117.

NASA (n.d.[a]). *Akatsuki Mission*. https://science.nasa.gov/mission/akatsuki/. Acedido em 1 março 2026.

— (n.d.[b]). *Mariner 10 Mission*. https://science.nasa.gov/mission/mariner-10/. Acedido em 1 março 2026.

NASA Jet Propulsion Laboratory (2024). *Horizons On-Line Ephemeris System*. https://ssd.jpl.nasa.gov/horizons/app.html/. Accessed: October 2025.

National Aeronautics and Space Administration (2025). *Venus: Facts*. NASA Science Web page. accessed on June 6th 2025. URL: https://science.nasa.gov/venus/venus-facts/.

Oyama, V. I. et al. (1980). "Pioneer Venus gas chromatography of the lower atmosphere of Venus". In: *Journal of Geophysical Research* 85.A13, pp. 7891–7902. DOI: 10.1029/JA085iA13p07891.

Peralta, J., R. Hueso, and A. Sánchez-Lavega (2007). "A reanalysis of Venus winds at two cloud levels from Galileo SSI images". In: *Icarus* 190, pp. 469–477. DOI: 10.1016/j.icarus.2007.03.028. URL: https://doi.org/10.1016/j.icarus.2007.03.028.

Piccialli, A. et al. (2008). "Cyclostrophic winds from the Visible and Infrared Thermal Imaging Spectrometer temperature sounding: A preliminary analysis". In: *Journal of Geophysical Research: Planets* 113, E00B11. DOI: 10.1029/2008JE003127.

Pollack, J. B., O. B. Toon, and R. Boese (1980). "Greenhouse models of Venus' high surface temperature, as constrained by Pioneer Venus measurements". In: *Journal of Geophysical Research* 85.A13, pp. 8223–8231. DOI: 10.1029/JA085iA13p08223.

Russell, C. T. et al. (2007). "Lightning on Venus inferred from whistler-mode waves in the ionosphere". In: *Nature* 450.7170, pp. 661–662. DOI: 10.1038/nature05930.

Sánchez-Lavega, A. et al. (2008). "Variable winds on Venus mapped in three dimensions". In: *Geophysical Research Letters* 35.13, p. L13204. DOI: 10.1029/2008GL033817.

Sánchez-Lavega, Agustín (2010). *An Introduction to Planetary Atmospheres*. 1st. Boca Raton, FL: CRC Press. ISBN: 978-1420067323. DOI: 10.1201/9781439894668.

Saunders, R. S. et al. (1992). "Magellan mission summary". In: *Journal of Geophysical Research* 97.E8, pp. 13067–13090. DOI: 10.1029/92JE01397.

Schubert, G. et al. (1980). "Structure and circulation of the Venus atmosphere". In: *Journal of Geophysical Research* 85.A13, pp. 8007–8025. DOI: 10.1029/JA085iA13p08007.

Sonett, C.P. (1963). "A summary review of the scientific findings of the Mariner Venus mission". In: *Space Science Reviews* 2, pp. 751–777. DOI: 10.1007/BF00208814.

Spacecraft and Vehicles (2025). *Akatsuki Venus Climate Orbiter (Planet-C)*. Online article on Spacecraft and Vehicles website. URL: https://spacecraftandvehicles.com/spacecraft/orbital/akatsuki-venus-climate-orbiter/.

Takagi, Masahiro (Mar. 2025). *Dynamics of the Venusian atmospheric superrotation*. Seminar at the Faculty of Sciences of the University of Lisbon. Lisbon, Portugal.

Taylor, F. W. (2006). "Climate Variability on Venus and Titan". In: *Space Science Reviews* 125.1, pp. 445–455. DOI: 10.1007/s11214-006-9077-y.

Taylor, F. W. et al. (1979). "Infrared remote sounding of the middle atmosphere of Venus from the Pioneer Orbiter". In: *Science* 203.4382, pp. 779–781. DOI: 10.1126/science.203.4382.779.

Titov, D. V. et al. (2008). “Atmospheric structure and dynamics as the cause of ultraviolet markings in the clouds of Venus”. In: *Nature* 456, pp. 620–623. DOI: 10.1038/nature07466.

Turcotte, D. L. (1995). “How does Venus lose heat?” In: *Journal of Geophysical Research* 100.E8, pp. 16931–16940.

Widemann, T., E. Lellouch, and A. Campargue (2007). “New wind measurements in Venus’ lower mesosphere from visible spectroscopy”. In: *Planetary and Space Science* 55.12, pp. 1741–1756. DOI: 10.1016/j.pss.2007.01.004.

Widemann, T., E. Lellouch, and J.-F. Donati (2008). “Venus Doppler winds at cloud tops observed with ESPaDOnS at CFHT”. In: *Planetary and Space Science* 56.10, pp. 1320–1334. DOI: 10.1016/j.pss.2008.07.005.

Williams, David R. (2024). *Venus Fact Sheet*. NASA Goddard Space Flight Center – NSSDCA. Última atualização em 11 de janeiro de 2024. URL: https://nssdc.gsfc.nasa.gov/planetary/factsheet/venusfact.html.

Young, A. T. (1975). “Is the Four-Day “Rotation” of Venus Illusory?” In: *Icarus* 24.1, pp. 1–10. DOI: 10.1016/0019-1035(75)90152-9.